Mineralogical Magazine, December 2005, Vol. 69(6), pp. 995–1018

Extremely Pb-rich rock-forming silicates including a beryllian scapolite and associated minerals in a skarn from Långban, Värmland, Sweden

A. G. CHRISTY[1] AND K. GATEDAL[2]

[1] Department of Earth and Marine Sciences, Building 47, Australian National University, Canberra, ACT 0200, Australia
[2] Mining Museum of Nordmark, SE-682 93 Nordmarkshyttan, Sweden

ABSTRACT

We report preliminary petrographic and mineral chemical data for a rock hosting an unusual mineral assemblage from Långban, Värmland, Sweden. The rock is a two feldspar-scapolite-spessartine-romeite skarn. The bulk composition and high degree of enrichment in Pb, Sb and As suggest that the rock was formed by reaction between a pre-existing Mn skarn containing the chalcophiles and a potassic granite, with loss of silica, alkalis and CO_2. The alkali feldspar is a Pb-rich hyalophane, averaging $Or_{63}Ab_{19}Cs_{15}Pb_{03}$, the plagioclase feldspar a Pb-rich labradorite, $An_{48}Ab_{48}Or_{02}Pb_{02}$, and the scapolite a 'mizzonite' (Ca/(Na+Ca) = 0.66–0.70). These minerals show their highest Pb contents recorded in nature to date: up to a maximum of 5.7 wt.% PbO in the hyalophane, 2.1% PbO in the plagioclase, and 5.3% PbO in the scapolite. Laser ablation ICP-MS of a scapolite grain detected substantial Be up to 1.7 wt.% BeO (0.6 Be per 12 tetrahedral cations), as well as Pb up to 7.05 wt.% PbO. The Be is incorporated into scapolite via the coupled exchange $[Be(OH)][Al(CO_3,SO_4)]_{-1}$. This is the first documentation of scapolite as the major repository for Be in a rock.

The romeite also contains substantial Pb, and shows extensive solid solution towards end-members containing Fe^{3+}, Ti and Sb^{3+}. In some analyses, the dominant end-members are $Ca_2(Fe^{3+}_{0.5}Sb^{5+}_{1.5})O_6(OH)$ and its Pb analogue rather than $(Ca,Pb)_2Sb_2O_7$. Complex exsolution textures are displayed in the hyalophane, by hancockite-epidote, romeite-bindheimite and hedyphane-johnbaumite. Ca-rich scapolite and hancockite appear to be new minerals for the Långban deposit.

The mineralogy appears consistent with the regional peak conditions of P = 3 kbar, T > 600ºC. Several potential thermobarometers for Mn-rich skarns are identified in this rock.

KEYWORDS: hyalophane (plumboan), plagioclase (plumboan), scapolite (beryllian and plumboan), romeite-bindheimite, hancockite-epidote, hedyphane-johnbaumite, skarn, Långban, Sweden.

Introduction

THE mines at Långban, Värmland, Sweden (59.86ºN, 14.27ºE; Fig. 1) have long been famous for the extreme diversity of their minerals and mineral associations (Moore, 1970; Holstam and Langhof, 1999). Approximately 300 mineral species have been described from this deposit, in which lenses of Fe or Mn oxide-rich ore are hosted by carbonates and siliceous volcanics of early Proterozoic age (~1.85 Ga) and regionally metamorphosed up to amphibolite facies. The oxides appear to have contained appreciable concentrations of As, Sb, Pb and Ba, elements that are major contributors to the mineralogical diversity developed subsequently, but relatively minor amounts of Cu, Zn and Bi. Reaction with pegmatitic fluids from younger granite intrusions subsequently introduced additional chemical

* E-mail: andyc@ems.anu.edu.au
DOI: 10.1180/0026461056960304

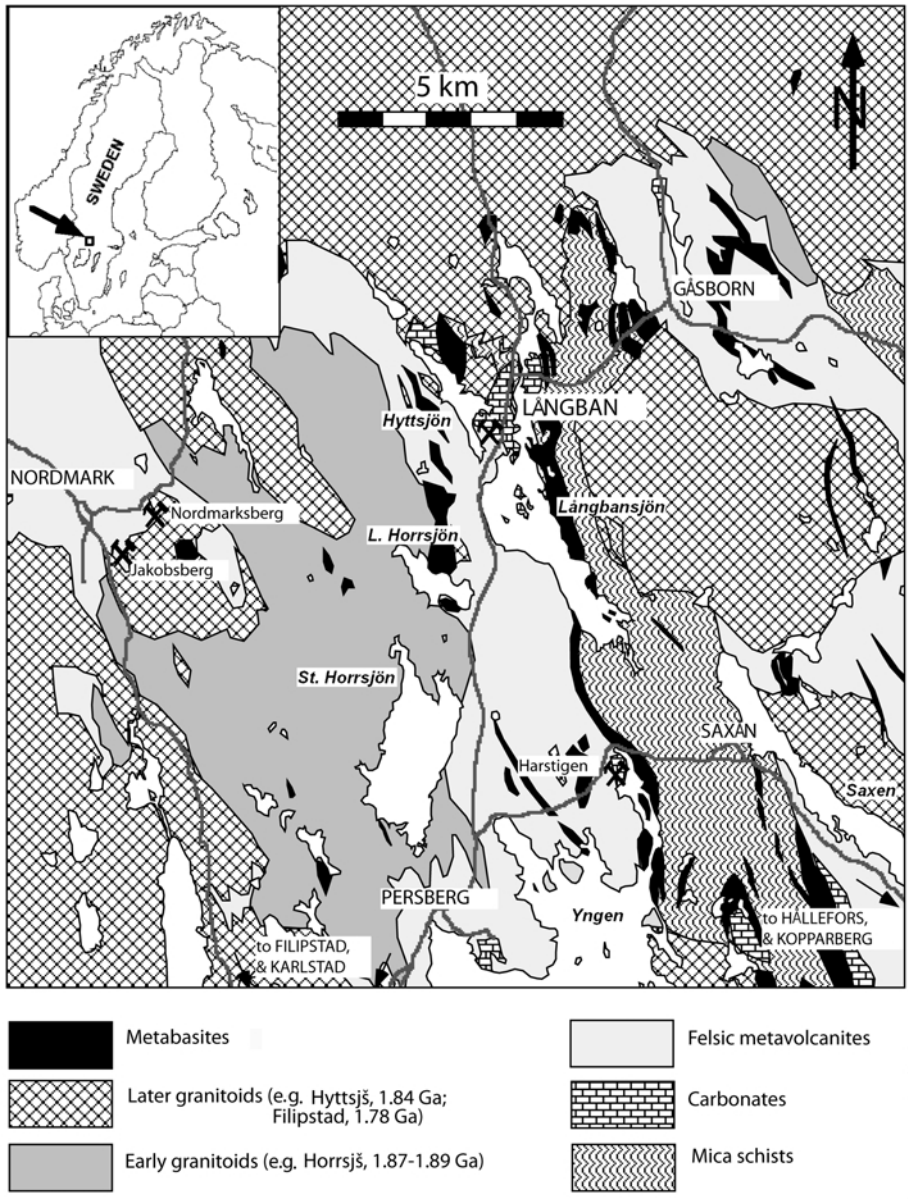

FIG. 1. Simplified geological map of the Långban area. Major towns, roads and lakes indicated on main map, along with Långban and some other Långban-type mines. Main map simplified after Sveriges Geologiska Undersökning Ser. Af nr 147, Berggrundskartan 11 E Filisptad NV.

components such as Be, F, Sn and W. The combination of this suite of elements with those of sedimentary-exhalative origin resulted in the crystallization of minerals such as swedenborgite ($NaSbBe_4O_7$), tilasite ($CaMgAsO_4F$), sverigeite ($NaMn_2Sn[Be_2Si_3O_{12}(OH)]$) and welinite ($(Mn_6(W,Mg)_2Si(O,OH)_7$) that are restricted to the Långban district or known from only a few other localities outside it.

Långban is unusual not just for new species, but also for the unusual chemical compositions of common species. In this paper, we report

preliminary petrographic and mineral chemical data for a new mineral assemblage in a rock from the Långban dumps in which major rock-forming minerals exhibit an extreme degree of solid solution towards Pb end-members. Scapolite containing significant Be as well as Pb is reported for the first time. Several species show exsolution textures implying the existence of solvus gaps. Some equilibria are identified which may be of use in geothermometry in complex skarns such as those at Långban, given modest amounts of additional thermodynamic data for some end-members and activity-composition data for solid solutions.

Petrographic description

The rock described in this study is a small hand specimen (~3 cm) collected with permission from the fenced area of the dumps at Långban by one of us (KG) in 2002. In hand specimen, it is a pale grey, apparently feldspathic rock with a millimetre-scale subhedral to anhedral granular texture. Initially, we regarded it as a 'syenite pegmatite'. Conspicuous minor minerals were a yellow-orange garnet in equant grains with rather ragged margins up to 3 mm in diameter, and sub-millimetre equant grains of a lustrous, dark brown mineral of the pyrochlore group. Detailed examination of the rock was prompted by the observation of radial cracking around some of these grains, in response to either differential thermal expansivity between oxide and silicate phases or to volume or compressibility change induced by a structural phase transformation.

Inspection under short-wave ultraviolet light revealed that the 'feldspar' comprised at least two phases, one that was brightly fluorescent yellow-white, in addition to one with only weak purple fluorescence. Since strong whitish fluorescence and grey, feldspar-like appearance are characteristic of the (Ba,Pb,Be,B)-bearing scapolite-group mineral hyalotekite (Christy *et al.*, 1998), small chips were analysed semi-quantitatively by energy-dispersive X-ray analysis (EDXA) on the JEOL 6400 SEM at the Electron Microscopy Unit, at ANU. The weakly fluorescent phase was confirmed as a K-feldspar with BaO and PbO well above their detection limits (plumboan hyalophane). The strongly fluorescent phase was not hyalotekite, but a calcium aluminosilicate with minor Pb but almost no Ba. Polished thin sections were made for further study by optical microscopy and SEM, including quantitative EDXA.

Hyalophane was the modally dominant mineral. The highly fluorescent silicate was visible as colourless subhedral prisms with a conspicuous sieve texture and showing second-order interference colours, and was identified as scapolite (Fig. 2). Some lamellar-twinned plagioclase was also present. The feldspars, particularly the plagioclase, showed some sericitic alteration. All feldspar grains were anhedral with sutured boundaries indicative of some post-growth deformation and recrystallization, with incomplete textural re-equilibration. This was also evident in the yellow garnets, which showed ragged margins. A few grains of several other mafic minerals were noted, including a pale yellow clinopyroxene, pale yellow epidote ragged prisms of a green-brown pleochroic clinoamphibole and plates of greenish pleochroic mica (Fig. 3) as well as clots of an opaque oxide. All were subhedral at best. The pyrochlore-group mineral was present as rounded octahedra, isolated and in small aggregates, isotropic and dark brown in the microscope. Small patches and lenses of calcite appeared to represent late hydrothermal alteration.

Examination by SEM using back-scattered electron (BSE) imaging and energy-dispersive X-ray (EDX) analysis revealed the presence of several other minerals. Skeletal aggregates tens of microns long of an apatite-group mineral were observed. High magnification revealed these to consist of a eutectoid intergrowth of two phases of different mean atomic number. Lamellae were typically ~5 μm wide. The heavy phase was close to ideal hedyphane in composition

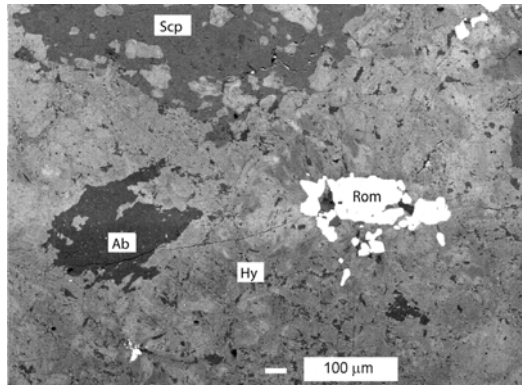

FIG. 2. BSEI showing exsolved albite (Ab) in a matrix of hyalophane (Hy), patchy contrast due to variation in content of Ba and Pb, and associated romeite (Rom) and scapolite (Scp).

($Pb_3Ca_2(AsO_4)_3Cl$) whereas the lighter phase was richer in Ca and P, and poorer in Cl. No F-$K\alpha$ peak was observed in EDXA, and selection of F for analysis gave negative apparent percentages. A few small grains were identified by EDXA as zircon, baryte and galena.

The BSE contrast was 'inverted' relative to most rocks in that in general, the felsic minerals scattered more strongly than mafic minerals due to their high Pb and/or Ba contents. Complex chemical zonation of these elements was apparent in the hyalophane and the epidote. The hyalophane was also revealed to have exsolved flames of nearly pure albite late in its history. The mafic minerals, even the garnet, showed very uniform BSE contrast, implying little or no zonation of major elements. However, small BSE-bright spots were observed near the rim of the clinopyroxene the composition of which suggested some exsolution of or alteration to a Pb-rich amphibole.

We note that spessartine-dominant garnet is stated to be 'rare' at Långban by Holtstam and Langhof (1999). Ca-rich scapolite and the Pb-rich epidote analogue, hancockite, appear to be new minerals for the Långban ore deposit. The overall mineral association represented by this rock is certainly new, as is the extremely high Be content of the scapolite and the Pb content of the rock-forming tectosilicates generally.

Mineral compositions

The majority of the analyses reported in this study were obtained on the JEOL 6400 SEM at the Electron Microscopy Unit, at ANU. This instrument is equipped with an Oxford Link ISIS EDX system employing an ATW thin window and Si(Li) solid state detector. The accelerating potential was 15 kV, beam current was 1 nA, the beam was focused to a spot ~3 μm in diameter, and spectra were collected for 3 min live time. Count rates were typically 3000 c/s (higher for compositions rich in heavy elements), and detection limits for the elements analysed were all ~0.1 wt.% oxide. The most abundant elements were quantified using the following standards, mainly from the ASTIMEX MINM2S-53 set: albite (Na-$K\alpha$, Al-$K\alpha$), periclase (Mg-$K\alpha$), sanidine (Si-$K\alpha$, K-$K\alpha$), fluorapatite (P-$K\alpha$), pyrite (S-$K\alpha$, Fe-$K\alpha$), tugtupite (Cl-$K\alpha$), diopside (Ca-$K\alpha$), rutile (Ti-$K\alpha$), manganese (Mn-$K\alpha$), arsenic (As-$L\alpha$), celestite (Sr-$L\alpha$), zirconolite (Zr-$L\alpha$), antimony (Sb-$L\alpha$), baryte (Ba-$M\alpha$), galena (Pb-$M\alpha$). Spectra were also checked for the presence of elements such as F and Bi, but these were rarely found to be above detection limit. The efficiency of the software at deconvolution of overlapping peaks was verified by analysis of the rutile standard and baryte standard with both Ba and Ti selected (Ba-L–Ti-K overlap) and diopside and stibnite with Sb and Ca selected (Sb-L–Ca-K overlap). Elements that were not physically present were below the detection limit in all cases.

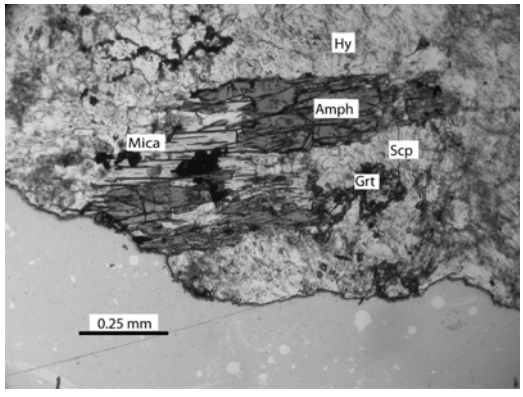

FIG. 3. Optical micrograph of mica, amphibole and garnet in a matrix that is predominantly hyalophane and scapolite. Dark grains in mica are romeite.

Hyalophane

The K-rich feldspar has very variable Ba and Pb contents (Table 1, analyses 3–8; Fig. 2). The Pb and Ba element maps revealed patchy inhomogeneities on the 100 μm scale, with no obvious preferred orientation. This texture may reflect incipient exsolution from an homogeneous high-temperature phase towards coexisting high-Pb, high-Ba and low-(Pb, Ba) phases at lower temperatures. Almost pure albite was also exsolved as flames and patches within the K-feldspar (Table 1, analyses 9–10; Fig. 2). Table 1 includes analyses derived from scanning approximately 1 mm^2 areas of single grains, to provide an indication of the composition of the homogeneous phase (analyses 1–2) as well as analyses obtained from 3 μm spots. The data selected for Table 1 are those with totals nearest 100% and cation:anion ratios near 5:8, selected from a total of 30 analyses. Others gave low totals (88–98%), presumably due to alteration. Some grains showed patches of turbidity with fine-grained inclusions, provisionally identified as clays, micas and calcite.

TABLE 1. Feldspar analyses.

	1 Kfsp-area	2 Kfsp-area	3 Kfsp	4 Kfsp	5 Kfsp	6 Kfsp	7 Kfsp	8 Kfsp	9 Alb	10 Alb	11 Plag	12 Plag	13 Plag
SiO_2	56.78	56.59	58.09	52.68	56.4	55.61	51.23	53.46	68.13	67.35	58.66	53.18	52.99
Al_2O_3	19.86	20.11	19.9	20.5	19.84	20.02	21.3	20.73	18.74	19.41	23.54	27.54	27.27
Fe_2O_3	n.d.	n.d.	0.11	0.15	0.06	n.d.	n.d.	n.d.	0.35	0.22	0.61	0.12	0.15
CaO	0.30	0.27	n.d.	0.55	n.d.	0.07	0.12	0.01	0.83	0.15	5.85	9.65	9.68
MnO	0.12	0.11	n.d.	0.09	0.03	0.12	0.10	n.d.	0.38	0.09	n.d.	n.d.	0.01
SrO	n.d.	n.d.	n.d.	n.d.	n.d.	n.d.	0.56	0.33	n.d.	n.d.	0.28	n.d.	n.d.
BaO	8.36	7.20	6.63	9.61	7.47	8.15	14.77	12.55	n.d.	0.21	n.d.	n.d.	n.d.
PbO	2.10	2.82	1.95	4.84	2.69	3.81	2.45	2.26	n.d.	0.42	1.64	2.12	2.08
Na_2O	1.87	2.06	2.41	1.71	1.27	1.69	1.59	1.79	11.87	11.22	8.13	5.33	5.20
K_2O	10.33	10.05	9.69	8.54	10.74	9.68	7.61	8.47	n.d.	0.44	0.11	0.12	0.38
Total	99.72	99.21	98.78	98.67	98.5	99.15	99.73	99.6	100.3	99.51	98.82	98.06	97.76
Cations per 8 oxygens													
Si	2.815	2.810	2.849	2.726	2.825	2.801	2.67	2.734	2.967	2.979	2.685	2.483	2.485
Al	1.161	1.177	1.15	1.250	1.171	1.189	1.308	1.249	0.962	1.012	1.270	1.516	1.507
Fe	–	–	0.004	0.006	0.002	–	–	–	0.011	0.007	0.021	0.004	0.005
Ca	0.016	0.014	–	0.03	–	0.004	0.007	0.001	0.039	0.007	0.287	0.483	0.486
Mn	0.005	0.005	–	0.004	0.001	–	0.004	–	0.014	0.003	–	–	–
Sr	–	–	–	–	–	–	0.017	0.010	–	0	0.007	–	–
Ba	0.162	0.140	0.127	0.195	0.147	0.161	0.302	0.252	–	0.004	–	–	–
Pb	0.028	0.038	0.026	0.067	0.036	0.052	0.034	0.031	–	0.005	0.020	0.027	0.026
Na	0.180	0.198	0.229	0.172	0.123	0.165	0.161	0.177	1.002	0.962	0.721	0.483	0.473
K	0.653	0.637	0.606	0.564	0.686	0.622	0.506	0.553	–	0.025	0.006	0.007	0.023
Total	5.020	5.019	4.991	5.014	4.991	4.994	5.009	5.007	4.995	5.004	5.017	5.003	5.005

Nos. 1–2 are area scans of 1 mm sized hyalophane grains. Nos. 3–8 are 3 μm points in hyalophane. Nos. 9–10 are exsolution flames of albite in hyalophane. Nos. 11–13 are plumboan oligoclase-labradorite.

Perthitic albite

Patches and flames of albite, up to several hundred microns in extent and very dark in BSE contrast, were clearly a late exsolution product from the hyalophane. Unlike the coarse plagioclase feldspar described below, this albite was essentially pure $NaAlSi_3O_8$ with no other components systematically present above detection limit (Table 1, analyses 9–10).

Plagioclase

The majority of the plagioclase is labradoritic in composition (~Ab_{47}) with some more sodic patches ranging to oligoclase (Ab_{72}). While Ba was rarely observed above detection limit on the SEM and did not exceed 0.9 wt.% BaO, Pb was always present at the level of 0.4–2.1 wt.% PbO, or ~0.5–2.7 mol.% $PbAl_2Si_2O_8$ component (Table 1, analyses 11–13). This is two orders of magnitude greater than the previously reported maximum Pb contents of natural plagioclase (170 ppm: Černý *et al.*, 1984; 400 ppm in the exsolved albite component of a perthite: Mason, 1982). The plagioclase showed more extensive low-temperature alteration than the hyalophane. Again, the alteration products are believed to be calcite and layer silicates.

Scapolite

Subhedral prisms of scapolite up to 3 mm long were colourless in plane light, but prominent in crossed polars because of their high birefringence. Interference colours ranged up to high third order. The scapolite grains exhibited sieve texture, being riddled with anhedral feldspar inclusions up to hundreds of microns across. This is apparent in Fig. 2. Cleavage traces were often visible.

Compared to the feldspars, the scapolite of this study was relatively homogeneous in major element composition (Table 2, analyses 1–6).

TABLE 2. Scapolite and epidote analyses.

	1 Scp	2 Scp	3 Scp	4 Scp	5 Scp	6 Scp	7 Epd	8 Epd	9 Hnk	10 Hnk
SiO_2	46.66	47.18	45.31	45.54	45.99	46.27	34.77	34.76	30.84	29.07
TiO_2	n.d.	n.d.	0.11	n.d.	0.04	n.d.	n.d.	0.10	0.23	0.19
Al_2O_3	22.81	22.13	23.39	23.22	22.70	23.33	20.03	20.24	17.27	15.9
Fe_2O_3	0.06	0.04	0.18	0.11	0.10	n.d.	13.77	14.44	13.09	13.69
MgO	n.a.	n.a.	n.a.	n.a.	n.a.	n.a.	0.06	0.11	0.33	0.17
CaO	14.99	15.31	15.34	15.21	15.29	14.67	19.03	19.46	13.29	11.71
MnO	0.08	0.11	0.23	0.16	0.08	0.09	0.63	0.60	0.59	0.55
SrO	0.99	1.18	0.86	0.65	0.79	0.51	0.42	n.d.	0.17	0.26
BaO	0.13	0.20	0.01.	0.26	0.02	0.14	0.03	n.d.	n.d.	n.d.
PbO	3.43	2.71	4.54	4.01	3.81	3.50	7.74	6.87	21.57	25.66
Na_2O	4.21	3.99	3.67	3.71	3.86	4.21	0.02	0.10	0.28	0.0
K_2O	0.22	0.33	0.20	0.27	0.15	0.19	n.d.	n.d.	n.d.	n.d.
P_2O_5	0.65	0.72	0.52	0.34	0.32	0.21	n.a.	n.a.	n.a.	n.a.
As_2O_5	0.36	0.55	0.48	0.47	0.33	0.39	n.a.	n.a.	n.a.	n.a.
SO_3	1.91	1.97	1.70	1.57	1.35	1.38	n.d.	n.d.	n.d.	n.d.
Cl_2O_{-1}	0.69	0.61	0.63	0.61	0.69	0.66	n.d.	n.d.	n.d.	n.d.
BeO*	1.68	1.77	1.41	1.28	1.48	0.97	–	–	–	–
CO_2*	1.15	1.76	1.89	2.14	1.93	2.49	–.	–.	–	–
H_2O*	0.30	0.20	0.18	0.14	0.19	0.07	1.72	1.74	1.54	1.47
Total	100.32	100.76	100.65	99.68	99.12	99.08	98.15	98.42	99.20	98.67
	Scapolites recalculated as described in text						Epidotes normalized to 12.5 O			
P	0.084	0.093	0.068	0.045	0.042	0.028	–	–	–	–
As	0.029	0.044	0.039	0.039	0.027	0.032	–	–	–	–
Si	7.145	7.218	7.045	7.136	7.181	7.260	3.023	2.992	2.994	2.971
Ti	–	–	0.013	–	0.005	–	–	0.006	0.017	0.015
Al	4.117	3.990	4.286	4.288	4.177	4.314	2.052	2.053	1.976	1.915
Fe^{3+}	0.007	0.005	0.021	0.013	0.012	–	0.896	0.935	0.956	1.053
Be	0.618	0.650	0.528	0.480	0.556	0.366	–	–	–	–
Mg	–	–	–	–	–	–	0.008	0.014	0.048	0.026
Ca	2.460	2.510	2.556	2.554	2.558	2.466	1.773	1.795	1.383	1.282
Mn	0.010	0.014	0.030	0.021	0.011	0.012	0.046	0.044	0.049	0.048
Sr	0.088	0.105	0.078	0.059	0.072	0.046	0.021	–	0.010	0.015
Ba	0.008	0.012	0.001	0.016	0.001	0.009	0.001	–	–	–
Pb	0.141	0.112	0.190	0.169	0.160	0.148	0.181	0.159	0.564	0.706
Na	1.250	1.183	1.106	1.127	1.169	1.281	0.003	0.017	0.053	–
K	0.043	0. 064	0.040	0.054	0.030	0.038	–	–	–	–
Total	16	16	16	16	16	16	8.005	8.016	8.049	8.031
$[CO_3]^{2-}$	0.241	0.368	0.400	0.457	0.412	0.533	–	–	–	–
$[SO_4]^{2-}$	0.219	0.226	0.198	0.185	0.158	0.162	–	–	–	–
Cl^-	0.231	0.204	0.214	0.209	0.236	0.227	–	–	–	–
OH^-	0.308	0.202	0.187	0.149	0.194	0.078	1	1	1	1

Hnk = hancockite. *Be, C and H in scapolite estimated as described in text. H_2O in epidotes assumed = 1.0 p.f.u.

The atomic Si/(Al+Si) ratio was 0.632−0.644, close to the conspicuous modal peak in the data compilation of Teertstra and Sherriff (1997). The ratio Ca/(Na+Ca) = 0.658−0.698, very similar to the corresponding ratio for all divalent and monovalent large cations: $M^{2+}/(M^{1+}+M^{2+})$ = (Ca + Pb + Sr +Mn + Ba)/(Na + K + Ca + Pb + Sr + Mn + Ba) = 0.670−0.713. Chlorine and S were low, at 0.58−0.69 wt.% Cl_2O_{-1} and 1.2−2.0 wt.% SO_3, respectively. The minor elements Ti and Fe were below or close to detection limit. Potassium was also low (0.15−0.44 wt.% K_2O), compared

to the dataset of Teertstra and Sherriff (1997), while Ba spanned the full range of their values up to 0.02 wt.% BaO. Minor elements that were inhomogeneously distributed but usually extremely high in this scapolite include Sr (SrO 0.5−1.2 wt.%; compare maximum literature value of 0.57%), P (P_2O_5 0.2−0.7 wt.%, cf. 0.25%), As (As_2O_5 0.2−0.8 wt.%) and particularly Pb (Pb 1.9−4.4 wt.%). The elements F and Sb were not detected by EDXA in the scapolite. Magnesium was near the detection limit, but was not analysed due to interference from As.

Recalculation of the scapolite analysis revealed some problems. The Si/(Al+Si) and $M^{2+}/(M^{1+}+M^{2+})$ ratios correspond to 7.46−7.73 Si and 2.63−2.79 M^{2+} per formula unit if Si + Al = 12 and $M^{1+} + M^{2+} = 4$. The sum of these numbers should be 9−10 for a viable charge-balanced scapolite, but is 10.25−10.46 for the scapolites of this study, suggesting that the true numbers of these cations are lower. Furthermore, in analyses of scapolite, the ratios of large-channel cations (Na+K+Ca+Sr+Pb+Mn) to tetrahedral cations were systematically >4:12. At first, it was assumed that this was due to the presence of small calcite inclusions in microfractures, but the same discrepancy was observed in a second dataset collected with great care taken to avoid inhomogeneities. It was deduced that the most likely cause was the presence of an unanalysed tetrahedral cation, probably one of the light elements Li, Be or B. One grain ~1 mm long in a thin section was analysed by laser ablation induction-coupled plasma mass spectrometry (LA-ICP-MS) in order to test this hypothesis. Given the paucity of trace element data for scapolite (none is presented by Deer *et al.*, 2004), a range of other elements was also analysed. The system used comprised a Laurin Technic Helex ablation cell, Lamba Physik Compex 110i Laser producing ArF^+ laser light at 193 nm, and a Varian Ultramass quadrupole ICP-MS. The laser was operated at 5 Hz repetition rate and ~60 mJ pulse energy, with a spot size of 150 μm. Three spots were analysed. The mass spectrometer analysed for 30 isotope masses with a dwell time on each of 10 ms and total cycle time of 0.72 s. About 30 cycles of background counts and 40 cycles of sample data were collected in 50 s, during which time the beam excavated ~20 μm into the sample, as estimated from interference colours. The external standard material was NIST 612 glass, and a nominal CaO content in scapolite of 15.14 wt.% was used as the internal standard. Species analysed were ^{7}Li, ^{9}Be, ^{11}B, ^{29}Si, ^{44}Ca, ^{45}Sc, ^{49}Ti, ^{55}Mn, ^{65}Cu, ^{66}Zn, ^{71}Ga, ^{72}Ge, ^{75}As, ^{85}Rb, ^{88}Sr, ^{89}Y, ^{90}Zr, ^{121}Sb, ^{133}Cs, ^{137}Ba, ^{139}La, ^{140}Ce, ^{141}Pr, ^{146}Nd, ^{147}Sm, ^{153}Eu, ^{157}Gd, ^{163}Dy, ^{166}Er, ^{172}Yb, ^{175}Lu, ^{178}Hf, ^{208}Pb, ^{209}Bi, ^{232}Th and ^{238}U. Data are presented in Table 3. Lithium, Sc, Cu, Ge, Zr, Th and rare earths heavier than Sm were below the detection limit. Boron was only present at 3−5 ppm, but very substantial Be was found, corresponding to 1.0−1.7 wt.% BeO, or 0.4−0.7 Be per 12 tetrahedral cations. This range of Be content is exactly that predicted as required to correct the ratio of large cations to tetrahedral framework cations. The grain analysed by laser ablation shows lower As and Sr than the other grains analysed by EDXA, but has high Pb (PbO up to 7.05 wt.%). This is consistent with some early microprobe analyses of scapolite (not presented here since P and As were not included

TABLE 3. Laser ablation trace element data for scapolite. Concentrations in ppm except where stated.

	1	2	3
Li	<17	<9	<7
Be (wt.% BeO)	1.44 (8)	1.72 (9)	1.98 (6)
B	3.8 (4)	3.4 (3)	4.6 (6)
Sc	<2	<2	<2
Ti (wt.% TiO_2)	0.008 (1)	0.009 (1)	0.007 (1)
Mn (wt.% MnO)	0.188 (5)	0.222 (8)	0.266 (9)
Cu	<3	<3	<3
Zn	117 (11)	206 (22)	155 (18)
Ga	26 (2)	27 (3)	25 (2)
Ge	<5	<4	<4
As	93 (8)	59 (8)	51 (5)
Rb	32 (3)	26 (2)	23 (2)
Sr	132 (3)	120 (4)	154 (3)
Y	4.9 (4)	1.2 (2)	3.2 (3)
Zr	<1	0.6 (2)	<0.3
Sb	280 (16)*	243 (18)*	215 (27)
Cs	11.9 (8)	6.3 (5)	9.1 (7)
Ba (wt.% BaO)	0.18 (3)	0.15 (2)	0.10 (1)
La	52 (2)	42 (2)	54 (2)
Ce	25 (1)	23 (1)	21 (1)
Pr	4.4 (4)	4.0 (4)	4.2 (3)
Nd	10.1 (14)	10.8 (15)	8.7 (13)
Sm	1.3 (4)	2.0 (6)	<1
Pb (wt.% PbO)	5.16 (18)	4.21 (15)	7.05 (22)
Bi	2.1 (3)	3.1 (5)	1.5 (3)
Th	<0.1	<0.3	0
U	0.74 (17)	4.5 (12)	0.58 (14)

* After subtraction of Sb spikes from romeite inclusions.

in the analysis) in which PbO attained 5.30 wt.%. Other interesting features of the trace element data are the extreme enrichment in light rare earths, such that La > Ce > Nd, and the exclusion of Th relative to U.

The final algorithm for recalculation of scapolite analyses assumed that all Na, K, Ca, Mn, Sr, Ba and Pb acted as large channel cations, while Be, Al, Si, P, Ti, Fe^{3+}, As were tetrahedral framework cations and S, Cl occurred in channel anions. Then: (1) channel cations were normalized to 4; (2) the difference between the tetrahedral cation total and 12 was taken to be Be; (3) the excess positive charge above 24 tetrahedral and channel cations was taken to be balanced by channel anions CO_3^{2-}, SO_4^{2-}, Cl^- and an unanalysed monovalent species, presumed to be OH^- (but possibly F^- or HCO_3^-); (4) All S was assumed to be present as SO_4^{2-} and Cl as Cl^-; (5) the residual anion charge was used to estimate CO_3^{2-} and OH^-.

Final totals, including calculated percentages for BeO, CO_2 and H_2O, were very close to 100% (Table 2).

Epidote group

Occasional grains of a pleochroic colourless-yellow mineral showing high second-order interference colours were observed. Analysis in the SEM confirmed these as plumboan epidote. Backscattered electron images (BSEI) revealed wedge-shaped Pb-poor and Pb-rich domains, respectively dark and bright in BSE (Fig. 4). Sharp boundaries between dark and bright regions, and an apparent bimodal distribution of chemical compositions, suggest that this is a result of exsolution into two distinct phases rather than continuous compositional zonation. The Pb-rich domains have Pb>0.5 p.f.u, hence presumably dominant on the *M*(2) site of the structure, and are therefore hancockite rather than plumboan epidote. Analyses of both Ca-rich and Pb-rich epidote phases are shown in Table 2, analyses 7–10. High Pb content in epidote, or a solvus between epidote and hancockite, do not appear to have been reported previously for Långban (Holtstam and Langhof, 1999) or similarly Pb-rich deposits such as Franklin (Dunn, 1995). The rock in this study appears to provide a first record for hancockite at Långban, although it is relatively common at the nearby Jakobsberg mine, another deposit of Långban type (Holtstam and Langhof, 1994).

Clinopyroxene

Microprobe analyses showed a few equant, rounded pale brown grains to be a very Mn-rich diopside. No major element zonation was apparent in BSE contrast, but a small area near the rim was rich in submicron inclusions. Although too small to analyse unambiguously, EDX spectra were consistent with these being Pb-rich amphibole. The pyroxene showed substantial Tschermak substitution with relatively high Mn and Zn contents (Table 4, analyses 1–2). A representative formula recalculated so as to balance charges is shown in Table 5. A large number of pyroxene end-members at >1 mol.%

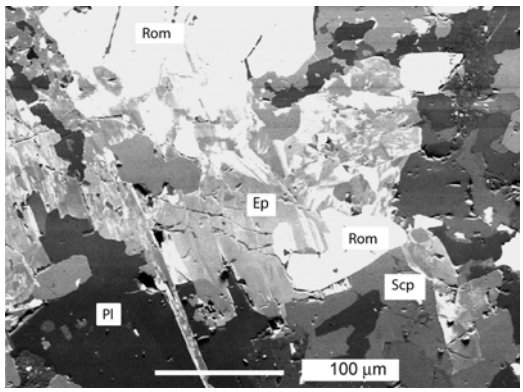

FIG. 4. BSEI showing epidote (Ep) exsolved into wedge-shaped Ca-rich (medium grey) and Pb-rich (white) domains. Also present are romeite (Rom), scapolite (Scp) and plagioclase (Pl).

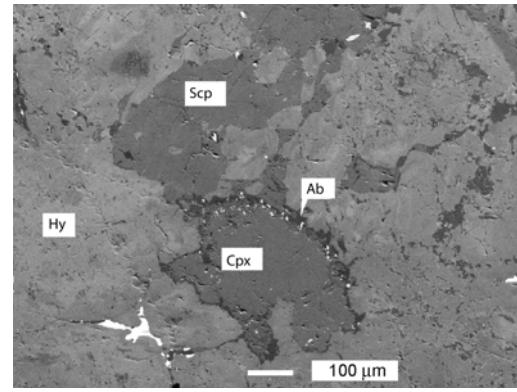

FIG. 5. BSEI of a clinopyroxene grain (Cpx) in a matrix of hyalophane (Hy) and sieve-textured scapolite (Scp). Note small hedyphane grains in hyalophane (white), albite selvage around pyroxene ('Ab', dark), and very fine-grained high-*Z* breakdown products in the pyroxene rim.

TABLE 4. Clinopyroxene, amphibole, mica and garnet analyses.

	1 Cpx (core)	2 Cpx (rim)	3 Amph	4 Amph	5 Mica	6 Grt
SiO_2	51.27	52.42	39.39	40.11	41.30	36.97
TiO_2	0.04	0.01	0.41	0.27	0.40	0.01
Al_2O_3	1.41	0.97	11.87	11.89	15.41	17.03
Fe_2O_3	5.90	5.83	12.64	12.28	6.02	7.76
MgO	11.99	12.84	12.91	13.24	21.32	0.93
CaO	21.25	20.99	11.14	11.44	0.33	12.78
MnO	6.76	5.76	2.93	2.43	1.03	24.63
ZnO	0.65	n.d.	n.d.	n.d.	n.d.	n.d.
SrO	n.d.	n.d.	0.25	n.d.	n.d.	n.d.
BaO	n.d.	n.d.	0.18	0.10	n.d.	n.d.
PbO	n.d.	n.d.	3.52	2.41	n.d.	n.d.
Na_2O	0.89	1.00	2.00	1.98	0.34	n.d.
K_2O	n.d.	n.d.	1.23	1.57	9.51	n.d.
H_2O*	–	–	1.98	2.00	4.27	–
Total	99.51	99.82	100.45	99.72	99.93	100.11
Cations per	—— 6 [O] ——		—— 23 [O] ——		11 [O]	12 [O]
Si	1.929	1.958	5.953	6.023	2.900	2.981
Ti	0.001	–	0.047	0.030	0.021	0.001
Al	0.063	0.043	2.114	2.104	1.275	1.619
Fe	0.167	0.164	1.437	1.388	0.318	0.471
Mg	0.673	0.715	2.908	2.964	2.232	0.112
Ca	0.856	0.840	1.804	1.841	0.025	1.104
Mn	0.215	0.182	0.375	0.309	0.061	1.682
Zn	0.018	–	–	–	–	–
Sr	–	–	0.022	0	0.010	–
Ba	–	–	0.011	0.006	–	–
Pb	–	–	0.143	0.097	–	–
Na	0.065	0.072	0.586	0.576	0.046	–
K	–	–	0.237	0.301	0.852	–
Total	3.987	3.975	15.637	15.639	7.731	7.970

*H_2O in amphiboles and mica assumed = 1.0 p.f.u.

TABLE 5. Representative charge-balanced and site-assigned formulae for major rock-forming minerals, based on average analyses.

Hyalophane: $(K_{0.63}Na_{0.19}Ba_{0.15}Pb_{0.03})[Al_{1.18}Si_{2.82}O_8]$

Plagioclase: $(Ca_{0.48}Na_{0.48}Pb_{0.02}K_{0.02})[Al_{1.50}Si_{2.50}O_8]$

Scapolite: $(Ca_{2.52}Na_{1.19}Pb_{0.13}Sr_{0.08}K_{0.04}Ba_{0.01}Mn_{0.03})[Be_{0.54}Fe^{3+}_{0.01}Al_{4.20}Si_{7.15}P_{0.06}As_{0.04}O_{24}](CO_3)_{0.40}\ Cl_{0.22}(SO_4)_{0.19}(OH)_{0.19}$

Clinopyroxene: $(Na_{0.07}Ca_{0.86}Mn^{2+}_{0.07})(Mn^{2+}_{0.14}Fe^{2+}_{0.03}Mg_{0.68}Zn_{0.02}Fe^{3+}_{0.13})[Al_{0.06}Si_{1.94}O_6]$

Amphibole: $(Na_{0.42}K_{0.24}Pb_{0.14}Sr_{0.02}Ba_{0.01}[]_{0.17})(Ca_{1.82}Na_{0.18})\ (Mg_{2.95}Fe^{2+}_{0.58}Mn_{0.38}Fe^{3+}_{0.88}Al_{0.16}Ti_{0.05})[Al_{1.98}Si_{6.02}O_{22}](OH)_2$

Mica: $(K_{0.88}Na_{0.05}Ca_{0.03}Sr_{0.01}[]_{0.03})(Mg_{2.29}Fe^{2+}_{0.33}Mn^{2+}_{0.06}Al_{0.30})[Al_{1.02}Si_{2.98}O_{20}](OH)_2$

Garnet: $(Mn^{2+}_{1.69}Ca_{1.10}Mg_{0.11}Fe^{2+}_{0.10})(Al_{1.63}Fe^{3+}_{0.37})[SiO_4]_3$

Epidote: $(Ca_{1.65}Pb_{0.36}Mn^{2+}_{0.05}Na_{0.02}Sr_{0.01})(Al_{2.00}Fe^{3+}_{0.97}Mg_{0.02}Ti_{0.01})[Si_2O_7][SiO_4]O(OH)$

are needed to express the composition of this solid solution. It can be expressed as $Di_{61}Jh_{14}Ae_{07}Kn_{07}Es_{06}Hd_{05}Pd_{02}$, where Di = diopside, Jh = johannsenite ($CaMnSi_2O_6$), Ae = aenigmatite, Kn = kanoite ($MnMgSi_2O_6$), Es = esseneite ($CaFe^{3+}AlSiO_6$), Hd = hedenbergite, Pd = petedunnite ($CaZnSi_2O_6$). Note there appears to be no significant octahedral Al, and hence negligible jadeite component, consistent with the relatively low pressures experienced at Långban (see below).

In addition to the exsolved grains of Pb-rich material, the clinopyroxene was surrounded by a narrow rim of albite (Fig. 5) which is discussed below.

Amphibole

A few ragged prisms of amphibole were observed, associated with yellow-brown pleochroic mica (Fig. 3). The amphibole was a grey-green colour in the γ direction (nearly ‖ crystallographic *z*, along the length of the prisms) and an orange-brown colour for light vibrating across the prisms. The measured extinction angles of 9–15º implied that this was the α colour (near crystallographic *x*) rather than the β colour (‖ *y*). Analyses are given in Table 4, with all Fe expressed as Fe_2O_3 prior to any recalculation. Table 4 shows a recalculation of an average amphibole formula to give 13 (*C*+*D*) cations {Mg, Fe, Mn, Al, Ti, Si} in $AB_2C_5D_8O_{22}(OH)_2$. The *B* sites were assumed to be occupied entirely by Na and Ca with no {Mn, Fe, Mg}, and Fe^{2+}/Fe^{3+} calculated so as to provide a total cation charge of +46.

The specific amphibole is a potassian, plumboan, manganoan magnesiohastingsite since $(Na+K)_A > 0.5$, $Ca_B > 1$, $Mg_C > Fe^{2+}_C$, $Fe^{3+}_C > Al_C$, $1.5 < Al_D < 2$. This analysis of a plumboan amphibole from Långban is similar to that by Gillberg (1960), also from Långban, but Pb and Fe are both higher in this study. The amphibole of Gillberg was a pargasite with 2.12 wt.%. PbO.

Mica

The mica associated with the magnesiohastingsite was a phlogopite (Table 4, analysis 5), pleochroic from nearly colourless (α) to grey-green (β/γ). In the more strongly absorbing directions, tan haloes were observable surrounding pyrochlore inclusions. This implied radiation damage from some U or Th content in the oxide mineral, but these elements were not observed above the detection limit. In contrast to the amphibole, Pb was below the detection limit in the mica.

Garnet

Large (up to 5 mm diameter) pale yellow porphyroblasts of garnet with irregular margins were the dominant ferromagnesian mineral in the rock. In contrast to the feldspars, epidotes and Sb-rich oxides (see below), the garnet crystals were extremely homogeneous in BSE images and EDX analyses, and showed no evidence of zoning. The garnet composition can be expressed as ~56 mol.% spessartine with subordinate andradite and grossular components (Table 4, analysis 6).

Pyrochlore group

The commonest oxide phase in the rock was a complex, Sb-rich member of the pyrochlore family, $A_2B_2O_6X$ with *A* = {Ca, Pb, Na, Sb^{3+} etc} 8-fold coordinated by oxygen, *B* = {Sb^{5+}, Ti, Fe^{3+}, etc.} in octahedral coordination and *X* = {O, OH, plus maybe F, H_2O, vacancies}. This mineral was presented as octahedral to anhedral grains, isolated in the silicate matrix or in small aggregates. The grains were isotropic in crossed polars. In plane light, there appeared to be two different generations of oxide. Most grains were dark red-brown in colour and rather turbid in appearance, while some others were golden yellow and devoid of inclusions (Fig. 6). The yellow grains often showed a marked octahedral parting, parallel to crystal faces; they also tended to be more euhedral, showing sharp corners rather

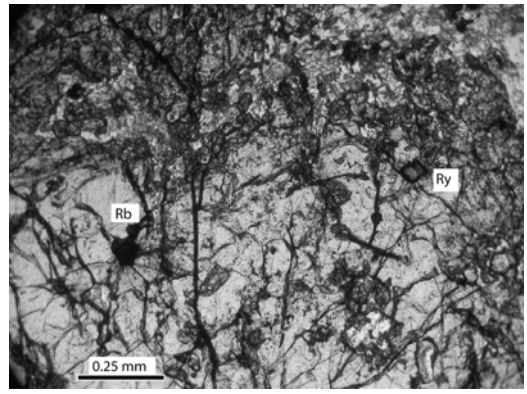

FIG. 6. Optical micrograph showing two generations of romeite grain included in large garnet. 'Rb' is a rounded, turbid brown grain with radial cracks around it. 'Ry' is an angular, transparent deep yellow grain.

than rounded ones, and overgrowth textures suggested that the yellow grains appeared to have grown later. Both yellow and brown grains were in some cases completely enclosed by large feldspar or garnet crystals, and hence appear to predate the major silicate phases.

Analyses for the pyrochlore-group mineral are shown in Table 6. Given the known chemical complexity of pyrochlore-group minerals, EDXA was initially used to screen grains for a wide range of elements which were considered to be possible minor-to-major element substituents. Cations that were usually above the detection limit (typically 0.1 wt.% oxide) were Na, Mg, Al, Si, Ca, Ti, Mn, Fe, As, Sr, Sb and Pb (Table 6). No significant K, Y, Zr, Nb, Ce, Ta, Bi, Th or U were detected. Antimony was consistently the dominant octahedral cation, and Ca was usually the dominant *A* cation. Hence, most of the pyrochlore group grains qualify as romeite (ideally $Ca_2Sb_2^{5+}O_6O$). Variable proportions of Ti and Fe (presumed ferric) were also assigned as octahedral, while the larger cations Na, Ca, Mn, Sr, Ba and Pb were assigned to the *A* sites of the pyrochlore structure. Assignment of Mn to the *B* sites resulted in a significant imbalance between the numbers of *A* and *B* cations.

It was found that in many cases, the Sb content was so high relative to other cations that, assuming all the Sb to be octahedral Sb^{5+} would

TABLE 6. Romeite-bindheimite analyses.

	1 Brown (core)	2 Brown (rim)	3 Brown (low Z, ppt)	4 Brown (high Z, ppt)	5 Yellow (core)	6 Yellow (rim)
As_2O_5	0.09	0.01	1.77	2.88	n.d.	0.28
Sb_2O_5	38.68	44.23	21.37	40.21	41.86	43.62
SiO_2	0.39	0.31	4.27	0.39	0.45	0.47
TiO_2	7.52	7.11	8.58	0.12	9.43	9.38
Al_2O_3	0.19	0.09	0.22	n.d.	0.27	0.27
Fe_2O_3	2.96	4.22	3.98	0.22	3.49	3.52
Sb_2O_3*	9.76	12.44	15.60	0.68	17.40	16.88
CaO	10.52	11.85	8.43	3.73	12.30	13.24
MnO	1.86	2.56	1.42	0.28	2.26	2.50
SrO	0.54	0.46	0.74	0.15	0.66	0.59
BaO	0.25	0.02	0.19	0.04	0.04	0.19
PbO	20.92	16.85	20.98	45.19	12.52	9.88
Na_2O	n.d.	0.30	0.02	0.16	n.d.	0.26
H_2O*	1.04	1.15	1.62	0.12	0.94	1.05
Total	94.72	101.60	89.18	94.17	101.62	102.13
Normalized to 2(As + Sb^{5+} + Si + Al + Fe), 4 cations and 7 anions						
As	0.004	–	0.081	0.176	–	0.011
Sb^{5+}	1.254	1.295	0.695	1.748	1.194	1.207
Si	0.034	0.024	0.374	0.046	0.035	0.035
Ti	0.494	0.421	0.565	0.011	0.545	0.526
Al	0.020	0.008	0.023	–	0.024	0.024
Fe	0.194	0.250	0.262	0.019	0.202	0.197
Sb^{3+}*	0.351	0.404	0.563	0.033	0.551	0.519
Ca	0.984	1.001	0.791	0.468	1.012	1.057
Mn	0.138	0.171	0.105	0.028	0.147	0.158
Sr	0.027	0.021	0.037	0.010	0.029	0.025
Ba	0.009	0.001	0.007	0.002	0.001	0.006
Pb	0.492	0.357	0.494	1.424	0.259	0.198
Na	–	0.046	0.003	0.036	–	0.038
OH^-*	0.604	0.603	0.947	0.097	0.481	0.522

* Sb^{3+} and H_2O calculated from stoichiometric constraints. K, Y, Zr, Nb, Ce, Ta, Bi, Th and U were also analysed but were below the detection limit.

result in extremely low cation totals per 7 oxygens. It was considered more likely that some Sb was in fact Sb^{3+} on the *A* sites, in which case it was possible to recalculate the formulae to 2 *A* and 2 *B* cations whilst simultaneously having the charge on the *X* anion position fall between −1 and −2, consistent with full occupation by (OH, O). Incorporation of the 'oxidizing' Fe^{3+} and 'reducing' Sb^{3+} cations in the same crystal structure is not problematic. The same combination of species is found in the minerals apuanite, ($Fe^{2+}Fe^{3+}_4Sb^{3+}_4O_{12}S$) and versiliaite ($Fe^{2+}Fe^{3+}_6Sb^{3+}_6O_{16}S$), which are polysomatic intermediates between schafarzikite ($Fe^{2+}_2Sb^{3+}_4O_8\square$) and a hypothetical end-member $Fe^{3+}_2(Fe^{3+}_2Sb^{3+}_2)O_8S$ (Mellini *et al.*, 1979; Mellini and Merlino, 1979). The original formulation of the mineral tripuhyite as $Fe^{2+}Sb^{5+}_2O_6$ would have provided an example of the incompatible combination Fe^{2+} and Sb^{5+}, but a recent re-examination of this species found the Fe to be oxidized, and led to its redefinition as disordered $Fe^{3+}Sb^{5+}O_4$ with the rutile structure (Berlepsch *et al.*, 2003).

The possibility of Sb^{3+} on octahedral *B* sites is discounted due to the stereochemical activity of its lone pair, which disfavours six close and symmetrical oxygen neighbours, as well as the relatively large size of Sb^{3+}: Shannon (1976) ionic radii for six-coordination by oxygen are 0.60 Å for Sb^{5+}, 0.605 Å for Ti and 0. 645 Å for high-spin Fe^{3+} but 0.76 Å for Sb^{3+}.

EDXA indicated that high-*Z* inclusions, up to 20 × 4 μm in size, observed in some grains still corresponded to Sb-rich pyrochlore compositions but had Pb > Ca, and may have represented low-*T* exsolution of a Pb-rich bindheimite $(Pb,Ca)_2Sb_2O_7$. Very small (5−10 μm) low-*Z* inclusions had appreciable Si, and may contain a silicate phase such as titanite (ideally $CaTiSiO_5$) rather than a pyrochlore phase. However, analyses would have included a considerable contribution

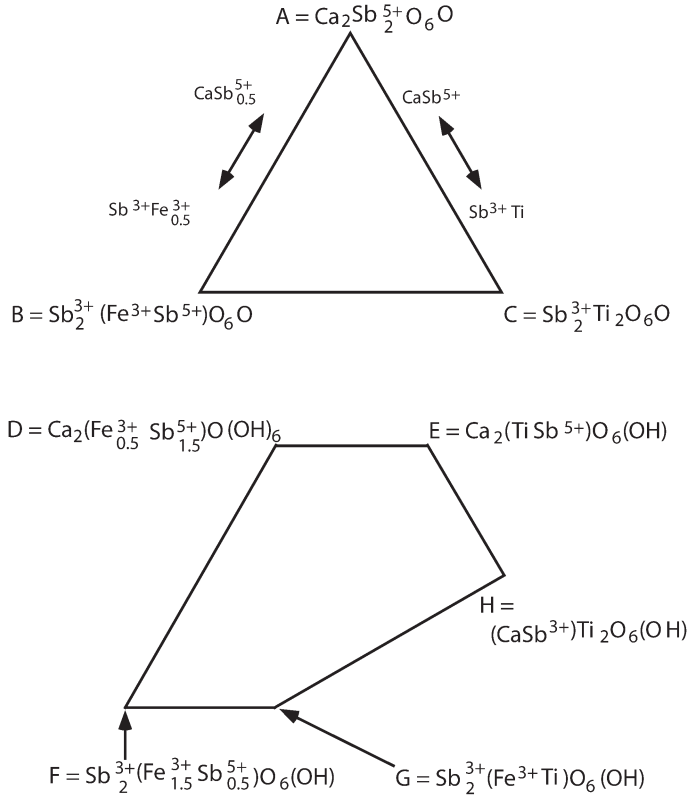

FIG. 7. Coupled solid solutions between Ca pyrochlore end-members for total cation charge = +14 (above) and +13 (below). The end-members indicated by letters are the vertices of a 3-dimensional polyhedron in the Ca-Fe-Ti-Sb-O-H system. The compositions of Fig. 8 all lie in the interior of this polyhedron, if Pb is included with Ca.

from pyrochlore surrounding any non-pyrochlore phases.

Fe-Ti oxide

The rare grains of Fe oxide were nearly pure hematite with just over 2 mol.% $FeTiO_3$ and much smaller amounts of $MnTiO_3$ and Al_2O_3 in solid solution.

Apatite group

Numerous small, colourless phosphate-arsenate grains were difficult to see in thin section, but detectable to the naked eye by their orange fluorescence under short-wave ultraviolet light, and obvious in BSE due to their high Pb content. At high magnification, grains were seen to be micron-scale two-phase intergrowths, eutectoid in texture (Fig. 9). The two phases were very different in BSE contrast. The brighter, Pb-rich phase was also rich in As and Cl. Some analysed compositions approached that of ideal hedyphane, $Pb_3Ca_2[AsO_4]_3Cl$. The darker phase was relatively enriched in Ca and P, depleted in Pb, As and Cl (Table 7, Fig. 10). Fluorine was not distinguishable in the energy-dispersive spectrum, hence it was deduced that this phase was a phosphatian johnbaumite, $Ca_5[AsO_4, PO_4]_3(OH)$ as shown in Fig. 9.

Discussion

Crystallization sequence

The distinctive minerals of the rock in this study did not crystallize simultaneously. The two generations of romeite both occur as inclusions in garnet and in feldspars, and clearly predate those silicates. It is not clear why two generations of pyrochlore-group mineral, very similar in composition, are present. The turbid brown grains, which are earlier, may be inherited from a precursor rock, prior to the introduction of alkalis and silica, while the yellow grains are a product of dissolution and reprecipitation. There is a compositional difference (see below), which is that the yellow grains are poorer in Pb, richer in Ti, richer in total Sb including a greater proportion of Sb^{3+}, and less hydrous (see below). Pb liberated by partial dissolution of the

TABLE 7. Apatite group analyses.

	1 Ca-rich	2 Ca-rich	3 Ca-rich	4 Pb-rich	5 Pb-rich	6 Pb-rich
P_2O_5	8.48	5.91	6.05	n.d.	0.73	0.08
As_2O_5	42.12	43.27	45.94	29.57	29.85	27.38
CaO	41.80	39.53	42.21	10.16	13.95	9.60
MnO	0.31	1.13	n.d.	0.33	0.10	n.d.
SrO	0.13	n.d.	0.06	0.13	n.d.	0.04
BaO	0.08	0.32	n.d.	0.04	0.42	0.14
PbO	8.08	4.58	2.66	58.87	49.18	55.69
Cl_2O_{-1}	0.47	2.36	1.52	2.47	2.57	2.37
H_2O*	1.31	0.61	0.74	n.d.	n.d.	n.d.
Total	102.77	102.28	102.35	101.57	101.77	99.90
	Normalized to 3(P + As)			5(Ca+Mn+Sr+Ba+Pb) atoms		
P	0.738	0.543	0.527	–	0.109	0.014
As	2.262	2.457	2.473	2.852	2.744	2.823
Ca	4.601	4.599	4.656	2.008	2.628	2.028
Mn	0.027	0.104	–	0.052	0.015	–
Sr	0.008	–	0.004	0.014	–	0.005
Ba	0.003	0.014	–	0.003	0.029	0.011
Pb	0.223	0.134	0.074	2.923	2.328	2.956
Cl	0.106	0.561	0.343	0.997	1.011	1.025
Cations	7.863	7.851	7.733	7.852	7.802	7.836

* H_2O calculated assuming that $(OH^- + Cl^-) = 1$ p.f.u.

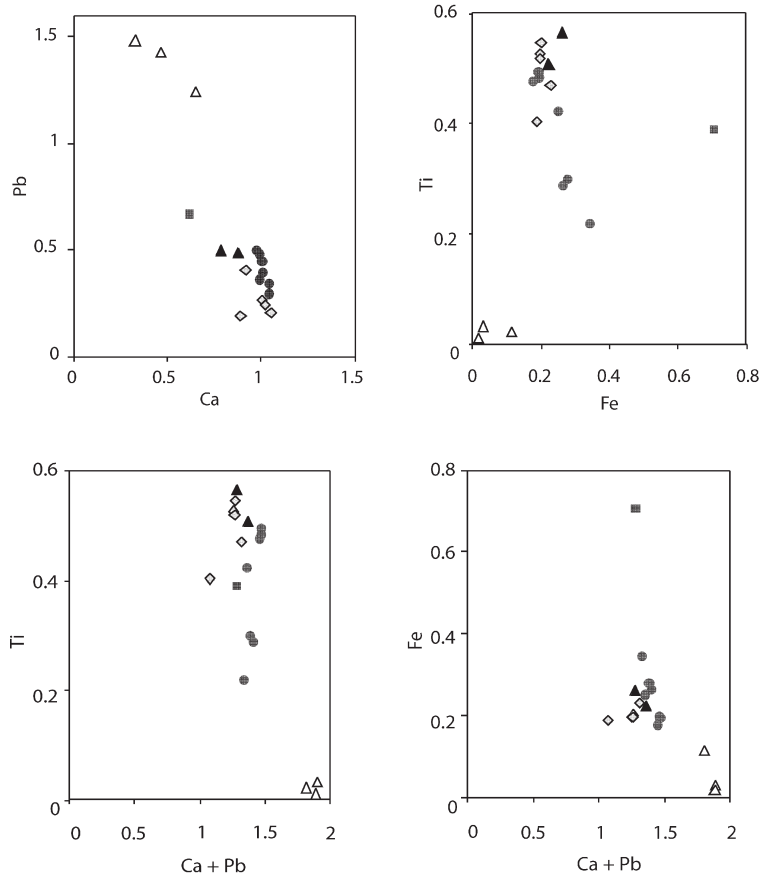

FIG. 8. Compositional variation of pyrochlore minerals. Brown grains (circles), yellow grains (diamonds), Fe-rich grain (square), low-Z inclusions (black triangles) and high-Z inclusions (open triangles) are distinguished.

brown grains may have been incorporated into the feldspars. Conversely, the Pb-rich apatite group minerals grew later than the feldspars. A Pb-depleted halo in the feldspar adjacent to hedyphane grains is conspicuous in BSEIs (Fig. 11), and implies that the feldspar was the source of the Pb in the arsenate-phosphate mineral. Feldspars can accommodate substantial P (cf. Černý *et al.*, 1984), and the same would be expected for As (same charge and similar size). The new feldspar group mineral filatovite (Filatov *et al.*, 2004; Vergasova *et al.* 2004) in fact approximates KAl_2SiAsO_8. It is thus possible that the P and As were also initially accommodated in feldspar along with Pb and Ca. A feasible reaction for producing hedyphane from a feldspar containing these elements that continues to react with an alkaline, SiO_2-rich fluid is:

$$\underset{\text{in feldspar}}{2CaAl_2Si_2O_8} + \underset{\text{in feldspar}}{3PbAl_2Si_2O_8} + \underset{\text{in feldspar}}{3\ KAl_2SiAsO_8} + \underset{\text{fluid}}{35SiO_2 + 13K^+ + 12OH^- + Cl^-} \rightarrow \underset{\text{hedyphane}}{Ca_2Pb_3[AsO_4]_3Cl} + \underset{\text{in feldspar}}{16KAlSi_3O_8} + 6H_2O$$

The garnet, scapolite, epidote and feldspars appear to be mutually contemporaneous. There is no evidence that this is untrue for the Mg-rich silicates (pyroxene, amphibole, mica) and hematite. However, very few pairs of these species are observed in mutual contact, given their scarcity. The coarse sieve texture of the scapolite, with its tubular inclusions of feldspar, is a disequilibrium texture that may be a consequence of very low interfacial energy between simultaneously crystallizing minerals, or may imply partial replacement of scapolite.

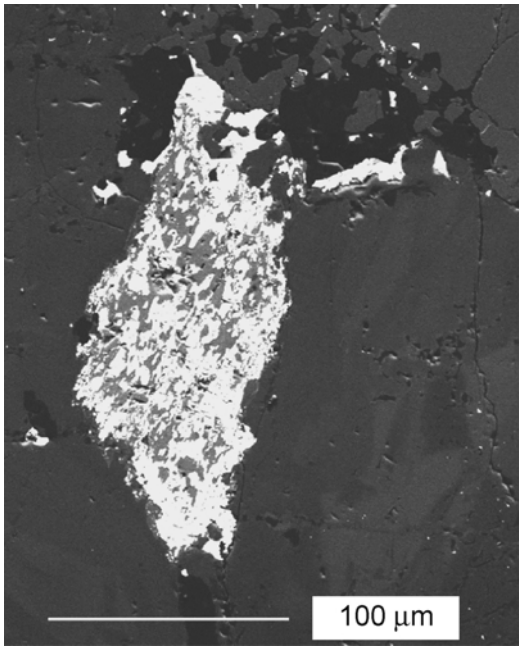

FIG. 9. BSEI showing eutectoid intergrowth of two apatite phases. The brighter phase is hedyphane, the darker phase is Ca-dominant and P-rich (phosphatian johnbaumite).

Calcite occurs only as small blebs at grain boundaries and in fractures, and is presumed to be retrogressive.

Compositional variation in hyalophane

The mean of the area scans (Table 1) has 18.9 mol.% $NaAlSi_3O_8$, 15.1 mol.% $BaAl_2Si_2O_8$, 3.3 mol.% $PbAl_2Si_2O_8$, 1.5 mol.% $CaAl_2Si_2O_8$ components. We deduce that the original homogeneous feldspar was close to this composition. On cooling, perthitic exsolution removed Na, while Ba and Pb segregated into patches that are richer in one or the other of these elements. The latter exsolution maintains optical continuity in crossed polars, and hence, is presumed to be structurally coherent.

Whereas comparable solution between K- and Ba-feldspars occurs widely, the Pb content of this feldspar exceeds that of any other reported natural mineral. The most Pb-rich 'amazonites' reported show 2.03% PbO at Portman Lake, Northwest Territories, Canada (Stevenson 1985; Stevenson and Martin 1986, 1988), and 1–2% from Broken Hill, New South Wales, Australia (Čech *et al.*, 1971; Plimer, 1976).

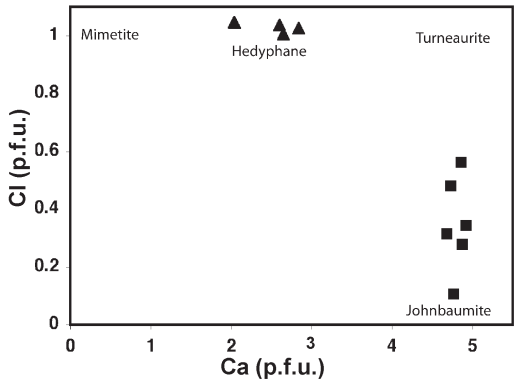

FIG. 10. Cl *vs.* Ca content for apatite-group analyses. As>>P in all cases, but Ca-rich analyses are systematically richer in P.

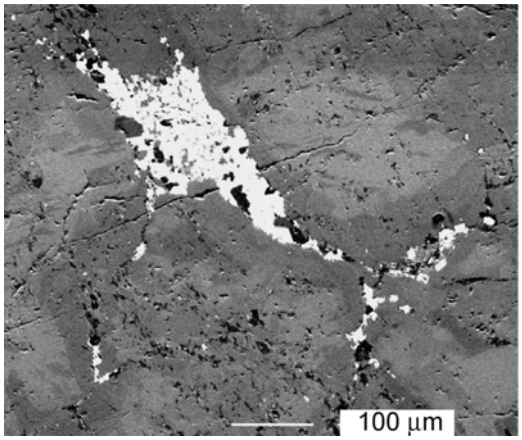

FIG. 11. BSEI of apatite-group eutectoid growing in hyalophane. Darker contrast in feldspar indicates a zone of Pb depletion surrounding hedyphane.

Scapolite

The scapolite solid-solution series is complex in that two distinct coupled exchanges, $(CaAl)(NaSi)_{-1}$ and $(CaCO_3)(NaCl)_{-1}$, operate between the two commonest end-members marialite ($Na_4[Al_3Si_9O_{24}]Cl$) and meionite ($Ca_4[Al_6Si_6O_{24}](CO_3)$). The relative importance of the two exchange vectors varies through the series, as does the extent and nature of Al-Si ordering (Levien and Papike, 1976; Teertstra and Sherriff, 1996, 1997; Sherriff *et al.*, 2000; Seto *et al.*, 2004). The macroscopic space group symmetry determined by X-ray diffraction varies

along the series and is $I4/m$ for the end-members but $P4_2/n$ for intermediate compositions (Papike and Zoltai, 1965; Papike and Stephenson, 1966; Lin and Burley, 1973*a*,*b*, 1975; Belokoneva *et al.*, 1993; Teertstra and Sherriff, 1996). However, transmission electron microscopic studies have also found the local symmetry to be as low as $P4$ or $P4/m$ for intermediate compositions (Phakey and Ghose, 1972; Hassan and Buseck, 1988). Hassan and Buseck attributed domain structures in Ca-rich scapolite to strong short-range ordering of interstitial clusters $[Ca_4(CO_3)]^{6+}$, $[NaCa_3(CO_3)]^{5+}$ and $[Na_4Cl]^{3+}$ coupled to framework Al-Si substitution. An intermediate mizzonite 'end-member' $NaCa_3[Al_5Si_7O_{24}](CO_3)$ was employed by Hassan and Buseck (1988) and also by Aitken (1983) in describing the scapolite series. However, Teertstra and Sherriff (1997) and Teertstra *et al.* (1999) avoided using it, since this precise composition has no special significance in terms of macroscopic symmetry, cation ordering or solid-solution trend. Teertstra and Sherriff (1997) classified the series into high-symmetry 'marialite' and 'meionite' and low-symmetry 'calcian marialite' and 'sodian meionite' divided at Ca/(Na+Ca) = 0.5. However, they do note that the 'mizzonite' composition appears to correspond to a stability maximum for the scapolite series, since such compositions are modally the most abundant.

An additional complication is that the CO_3^{2-} anion can be replaced by SO_4^{2-} in solid solution towards the silvialite end-member $Ca_4[Al_6Si_6O_{24}](SO_4)$ (Teertstra *et al.* 1999). This substitution is expected to increase towards high-pressure, high-temperature conditions, where the end-member is stable (Newton and Goldsmith, 1976; Goldsmith and Newton, 1977).

The scapolite of this study has $M^{2+}/(M^{1+} + M^{2+})$ very close to that of the maximally stable 'mizzonite' composition, but also contains significant amounts of silvialite component, probable hydroxide, Be and Pb. The latter two elements have not been recorded previously as substantial minor constituents of scapolite. Their occurrence in the scapolite of this study provides a chemical as well as structural similarity to the mineral hyalotekite, $(Ba,Pb,K)_4(Ca,Y)_2(B,Be,Si)_4Si_8O_{28}F$, which has its type locality at Långban (cf. Christy *et al.*, 1998). However, scapolite differs from hyalotekite in its low contents of Ba, Y and B.

The scapolite analyses of Table 2 and others show only slight Si enrichment relative to the trend of Si *vs.* (Na+K) plotted in Teertstra and Sherriff (1997). Therefore, it seemed unlikely that Be is incorporated via the exchange $(BeSi)(AlAl)_{-1}$, well known for other silicate minerals such as sapphirine-khmaralite (Christy *et al.* 2002; Christy and Grew, 2004). In order to identify which other coupled substitutions are active, the Be content estimated from apparent tetrahedral cation deficiency was plotted against Si, Al, (Na+K), (Cl+OH) and Cl for the analyses of Table 2 and others. The slopes of the regression lines were −0.148 (r^2 = 0.070), −0.898 (r^2 = 0.690), +0.132 (r^2 = 0.140), +1.199 (r^2 = 0.806), and +0.012 (r^2 = 0.019), respectively. It is clear that the exchanges $(BeSi)(AlAl)_{-1}$ and $(CaBe)(NaAl)_{-1}$ are unimportant in scapolite, but that the dominant exchange involves Al and the unanalysed monovalent anion, and is of the form $[Be(OH)][Al(CO_3,SO_4)]_{-1}$. This incorporation mechanism differs from any of those discussed in Grew (2002), and appears to be new. The maximum extent of this substitution is one Be atom per 12 tetrahedral cations, which implies that the most Be-rich compositions of this study show >50% of the maximum possible Be content. If this Be is strongly ordered onto 1 site p.f.u., these compositions may qualify as a new mineral species, but this is dependent upon the results of crystal-structure determination.

The incorporation of large amounts of Pb and particularly Be into scapolite is likely to extend considerably its stability field and range of associated minerals. The dramatic effect of similar contents of Be on the stability of sapphirine + forsterite is demonstrated by Christy and Grew (2004).

There is no evidence from apparent deviations in stoichiometry that any other minerals in the rock contain Be at concentrations as high as the scapolite. Even sodic plagioclase, in which Be is moderately compatible (Grew, 2002) can contain up to ~200 ppm in Be-rich pegmatites (Steele *et al.* 1977, cited and discussed by Smith and Brown, 1988; Kalt *et al.* 2001). However, we note that Grew (2002) gives the highest recorded Be content in scapolite as 37 ppm. Since the scapolite of the current study has Be two orders of magnitude higher than that, the Be contents of other minerals in this rock may also be unusually high.

Scapolite, like sapphirine and cordierite, is a rock-forming mineral that is normally low in Be but can evidently act as a repository for the majority of Be in the rock. In this rock, scapolite

as the Be-rich phase replaces the minerals containing essential Be such as barylite ($BaBe_2Si_2O_7$), bergslagite ($CaBeAsO_4OH$), bromellite (BeO), swedenborgite ($NaSbBe_4O_7$) and trimerite ($CaMn_2[Be_3Si_3O_{12}]$) that are typical of the Långban deposit. We expect Be-rich scapolite to play a similar role elsewhere in high-grade metamorphic rocks that are rich in Ca, Al and carbonate as well as Be.

Albite selvage around clinopyroxene

Two possible deductions from the albite selvage developed between hyalophane and clinopyroxene are: (1) that some jadeite component exsolved on depressurization, or (2) that the clinopyroxene had ceased to be stable in contact with K-rich feldspar and Ca-rich scapolite. The former possibility is unlikely given that pressures greater than those of the andalusite stability field were not experienced at Långban. However, the exact nature of any reaction between K-rich feldspar and clinopyroxene remains problematic. One possibility is that the albite selvage remains after the K-feldspar component of the hyalophane and the {Mg,Fe,Mn} of the pyroxene react to produce phlogopite mica, which crystallizes elsewhere. Since clinopyroxene and feldspar are relatively Si-rich but the only other K-rich mineral, phlogopite mica, is Si-poor, such a reaction cannot be balanced for Si without assuming that much Si is removed from the system:

$$\underset{\text{K-feldspar}}{KAlSi_3O_8} + 3CaMgSi_2O_6 + 3CO_2 + H_2O \rightarrow \underset{\text{phlogopite}}{KMg_3AlSi_3O_{10}(OH)_2} + \underset{\text{calcite}}{3CaCO_3} + \underset{\text{fluid}}{6SiO_2}$$

It will be seen later that the bulk composition of the skarn strongly suggests that there has been large-scale loss of silica from the system, which lends credence to this possibility.

Pyrochlore group

Pyrochlore-group nomenclature is problematic. In addition to romeite and bindheimite, we note that there are other names in the literature for {Ca, Pb, Sb, Ti, Fe}-rich pyrochlores, which are 'grandfathered-in' and, if not positively approved, are at least not formally discredited by the International Mineralogical Association (http://www.minda-t.org). 'Lewisite' has been used to refer to {Ca-Ti-Sb} pyrochlore from several localities, although none as yet in the Långban area. 'Monimolite', a known Långban mineral, appears from the crystallographic data to be a {Pb-Fe-Ti-Sb} pyrochlore, although the formula unit usually quoted is inconsistent with pyrochlore stoichiometry. Holtstam and Langhof (1999) state that monimolite is probably identical to bindheimite, although many old 'monimolite' specimens were found to be romeite on re-examination. In the absence of consistent definitions for these minerals, the pyrochlore compositions of this study are assigned as romeite (Ca-dominant on *A* sites, Sb on *B* sites), bindheimite (Pb on *A* sites, Sb on *B* sites), or not yet unambiguously named (other end-members dominant). A subcommittee of the International Mineralogical Association is currently reviewing pyrochlore nomenclature (http://sheba.geo.vu.nl/users/ima-cnmmn/imareport.htm), which should ultimately provide authoritative guidelines for the naming of ambiguous compositions.

We differ from Brugger *et al.* (1997) but concur with Rouse *et al.* (1998) that mixed-valence Sb partitioning as Sb^{3+} on the *A* cation sites and Sb^{5+} on the *B* sites is important in romeite-bindheimite-lewisite-type minerals. Much of the solid solution in the pyrochlore minerals involved predominantly end-members of the form $Ca_2Sb^{5+}_2O_7$–$Sb^{3+}_2(Fe^{3+}Sb^{5+})O_7$–$Sb^{3+}_2Ti_2O_7$ (anhydrous) and $Ca_2(Fe^{3+}_{0.5}Sb^{5+}_{1.5})O_6(OH)$–$Ca_2(TiSb^{5+})O_6(OH)$–$Sb^{3+}_2(Fe^{3+}_{1.5}Sb^{5+}_{0.5})O_6(OH)$–$(CaSb^{3+})Ti_2O_6(OH)$–$Sb^{3+}_2(Fe^{3+}Ti)O_6(OH)$ (hydrous). These compositions are 'end-members' in the sense of Hawthorne (2002) in which coupled substitutions result in occupation of only one site by two species. The ideal end-member formula for romeite is generally considered to be $Ca_2Sb^{5+}_2O_7$, but we note that Matsubara *et al.* (1996) described a natural pyrochlore in which $NaCaSb_2O_6F$ was the dominant end-member, and ascribed the name 'romeite' to this composition; this usage was questioned by Jambor and Roberts (1997). The other end-members of this study are un-named, hence letters *A*–*H* are used to identify them in Fig. 7, which illustrates the coupled substitutions between them. End-members *A* and *E* are related by the exchange vector $(TiOH)(Sb^{5+}O)_{-1}$. The pairs *A*–*D* and *B*–*F* are related by $(Fe^{3+}_{0.5}OH)(Sb^{5+}_{0.5}O)_{-1}$, and *C*–*G* by $(Fe^{3+}OH)(TiO)_{-1}$. There is a possibility of additional substitution towards cation-deficient or anion-deficient compositions such as $(Sb^{3+}\square)Sb^{5+}_2O_6(OH)$ or $Ca_2Ti_2O_6(\square, H_2O)$, but the proportions of such substitutions appeared to

be small in the minerals of this study. It was always possible to calculate charge-balanced formulae on the assumption of full occupancy of sites. Additionally to the coupled substitutions indicated, the only other significant type of compositional variation is the isovalent exchange $PbCa_{-1}$.

Analyses from the pyrochlore grains were classified into one of five groups: (1) brown grain matrices, (2) yellow grains, (3) high-*Z* inclusions in brown grains, (4) regions including small low-*Z* inclusions in brown grains, and (5) one 30 μm grain in a patch of similar-sized grains intergrown with hematite. The analyses of Table 5 include two examples of each of groups 1 and 2 and one each of groups 3 and 4. Major cations are shown in the plots of Fig. 8 for these analyses and twelve others. The following conclusions are drawn concerning the compositional variation in the pyrochlore minerals of this study.

(1) The brown grains show almost constant (Ca+Pb) content, but Ti plots against Fe to give a linear trend of slope approximately −2. There is, therefore, considerable substitution $Ti_2(FeSb)_{-1}$ in the brown grains.

(2) The yellow grains have very similar Ca and Fe contents to the brown, but are in general lower in Pb and Sb^{5+}, higher in Sb^{3+} and Ti. This suggests that the major differences between brown and yellow grains can be described in terms of $(Sb^{3+}O)(PbOH)_{-1}$ and $(TiOH)(Sb^{5+}O)_{-1}$ exchanges. The former is dominant, so the yellow grains are less hydrous than the brown, as well as having Sb in a lower mean oxidation state. The range of Fe content is much less in the yellow grains, although they lie on the same Fe-Ti trend as the brown. The Ca/Pb ratio tends to be slightly higher in the yellow grains than in the brown, due to the lower Pb content.

(3) If Si and other minor components are omitted, the low-*Z* inclusions and immediate environments are seen to lie at the Pb- and Ti-rich extremes of the composition range for the brown grains, with no clear compositional break. They are similar in Ti content to yellow grains, but much richer in Pb.

(4) The high-*Z* inclusions are quite separate in composition from all other analyses, with very high (Ca+Pb) and Pb >> Ca, making them bindheimite rather than romeite.

(5) The Fe-rich analysis is similar in (Ca+Pb) and Ti content to all others except the high-*Z* inclusions. The additional Fe appears to be incorporated predominantly by the substitution $(Fe^{3+}_{0.5}OH)(Sb^{5+}_{0.5}O)_{-1}$.

Dominant end-members (identified by the letters of Fig. 7) are *A* and particularly its Pb analogue in the high-*Z* inclusions, *A* with considerable substitution towards *B* and *C* in the brown and yellow grains and around the low-*Z* inclusions, but *D* and its Pb analogue in the high-Fe grain, which appears to have a lower total cation charge and hence is probably much more hydroxylated.

Bulk composition of rock

The sample was too small, and contained too much heavy elements, for routine analysis by X-ray fluorescence. The bulk composition was estimated by determination of modal abundances of the major minerals. The identity of the mineral species was ascertained at each of 500 random points in the thin section, and volume percentage modes determined from the point count. Since the minerals vary in density by a factor of 2, it was necessary to weight the volume modes according to approximate mineral densities in order to obtain weight percentages. The compositions of Table 4 were used for the minerals included in that table. Average hedyphane (apatite group) compositions were taken to be the means of the analyses quoted in Table 7. The romeite composition used was the mean of analyses 1 and 2 in Table 5, since the brown crystals greatly outnumbered the yellow. The hematite composition used included 4 mol.% ilmenite, 1 mol.% pyrophanite and 1 mol.% corundum. Densities to the nearest 0.1 g/cm^3 were estimated from the species data in the WWW database of Barthelemy (2000), except that of $PbAl_2Si_2O_8$ feldspar, not known as a dominant end-member in nature, which was calculated from the data of Benna *et al.* (1996). Modal abundance data are reported in Table 8. These were then used in conjunction with the compositional data to obtain the bulk composition estimate in Table 9. Percentages are relatively insensitive to the low precision of the density estimates. For example, reducing the assumed density for hyalophane to 2.75 g/cm^3 (1.8% relative change) reduces the wt.% mode for this mineral by a relative change of 0.6%, and the calculated wt.% K_2O and SiO_2 by 0.6% and 0.2%, respectively. Since hyalophane is low in density, by far the most abundant mineral in the rock, and the major repository for K and Si, these dependencies on density are likely to be greater than for other minerals.

TABLE 8. Modal abundance of minerals from point count.

Mineral	Vol.%	Density (g cm^{-3})	Wt.%
Hyalophane	70.0	2.8	66.1
Plagioclase	3.2	2.6	2.8
Scapolite	13.2	2.7	12.0
Epidote	1.8	4.0	2.4
Garnet	5.6	4.1	7.7
Clinopyroxene	0.6	3.2	0.7
Amphibole	0.4	3.2	0.4
Mica	0.2	2.8	0.2
Hedyphane	0.8	4.7	1.3
Romeite	2.6	5.1	4.5
Hematite	0.6	5.2	1.1
Calcite	1.0	2.7	0.9

The extremely high content of normally trace components such as BaO, PbO and As_2O_5, Sb_2O_5 renders it impossible for the rock to have originated as even a highly differentiated pegmatitic melt, despite its superficially syenite-pegmatitic appearance. The heavy elements would already have been concentrated in non-igneous precursor materials, and are known to be elevated in the Mn and Fe ores and skarns at Långban. The typical analyses tabulated in Holtstam and Langhof (1999) show BaO reaching 1.08% in the hausmannite ore, which also has 8–10% Pb and 400 ppm Sb as well as 72.5% MnO + Mn_2O_3. Arsenic appears to be most concentrated in Mn-rich skarns, where it reaches 1700 ppm ($\equiv$0.26% As_2O_5). Holtstam *et al.* (1998) regarded all the Mn, Ba, Pb, As and Sb of their skarns as original components of the volcanosedimentary sequence in the Långban area rather than being introduced during subsequent metamorphism. The rock in this study differs from the host rocks of the Sb minerals of Holtstam *et al.* in that feldspars and a feldspathoid rather than calcite are modally dominant. The very high Sb content of our romeite also leads us to deduce that Sb^{3+} is present in significant amounts along with Sb^{5+}, which contrasts with the conclusions of Holtstam *et al.* (1998) about Långban-type deposits, and Perseil and Smith (1995), Smith and Perseil (1997), Brugger *et al.* (1997) about other Mn-Sb skarns. The change in redox state of Sb in the rock of this study may reflect the much greater degree of interaction in this case between mineralized carbonate country rock and igneous precursors.

TABLE 9. Bulk composition estimated from mineral modes.

Component	Wt.%
SO_3	0.20
P_2O_5	0.12
As_2O_5	0.46
Sb_2O_5	1.92
Sb_2O_3	0.51
SiO_2	49.33
TiO_2	0.30
Al_2O_3	18.91
Fe_2O_3	2.06
FeO	0.16
BeO	0.17
MgO	0.25
CaO	4.98
MnO	2.12
SrO	0.13
BaO	5.18
PbO	3.65
Na_2O	1.97
K_2O	6.70
Cl_2O_{-1}	0.11
CO_2	0.63
H_2O	0.14
Total	100.00

The major element chemistry of the rock of this study differs from the Mn-rich rock analyses of Holtstam and Langhof (1999) in its high Na_2O content (2.0% as opposed to 0.1%), K_2O (6.7% *vs.* 0.1–1.8%), Al_2O_3 (18.9% is higher than even the metabasites at 14.9%; typical Mn skarns have 2.3%), and SiO_2 (near 50% as opposed to 4–11% in Mn skarns and ores). The implication is that the rock of this study has formed by reaction of metasediments, rich in Mn, As, Sb, Ba and Pb with a pegmatitic fluid that has introduced essentially all the Na, K, Al and Si in addition to Be. The very low Mg content excludes an ultramafic or mafic precursor. The high atomic K/Na ratio (2.18) suggests that the source for the fluid was a potassic granite, typical for the Baltic Shield in the Proterozoic. This ratio is compatible with values of 1.53–2.32 calculated for the Finnish granites tabulated by Carmichael *et al.* (1974). However, the elemental ratio Al/(K+Na) is much higher than for the Finnish granites (1.79 as opposed to 1.16–1.24), as is Al/Si (0.45 *vs.* 0.19–0.21). To produce the observed rock, reaction of Mn skarn with a pegmatitic fluid

possessing the (Na+K):Al:Si stoichiometry of a potassic granite would require some of the pegmatite's initial content of alkalis and much of its silica to be lost, presumably to an aqueous phase.

Pressure-temperature estimation

The conditions of formation of the Långban skarns are reviewed in Holtstam and Langhof (1999). The absence of kyanite, but the presence of cordierite, andalusite and sillimanite in associated metavolcanic rocks indicates $P < 3.5$ kbar, $T > 600$ºC. A high temperature is also suggested by the occurrence of periclase or periclase pseudomorphs in some marbles and the absence of a solvus gap in the kentrolite–melanotekite series, $Pb_2(Fe^{3+},Mn^{3+})_2[Si_2O_7]O_2$ ($T > 525$ºC: Lindqvist and Charalampides, 1987). Crude temperature estimates from the mineral compositions of the rock in this study are consistent, although the unusual bulk composition of the rock and mineral compositions make it challenging to find applicable thermobarometers for estimation of crystallization conditions. In particular, the very high Fe^{3+}/Fe^{2+} ratio, high proportion of Mn among divalent cations, and high proportion of non-classical Ba, Pb and Sr end-members in the feldspars all serve to render any simple activity model suspect. The maximum Ba content observed locally in the hyalophane ($X_{Ba} = 0.30$) is far higher than the data compiled by McSwiggen *et al.* (1994), implying $T >> 530$ºC.

We now consider examples of equilibria that could be considered in an attempt to obtain *P-T* estimates. The symbols are those recommended by the International Mineralogical Association (1998) and are: Ab, An and Kfs for the obvious feldspar end-members; Di, Ae and Es for diopside, aegirine and esseneite in clinopyroxene; Adr, Grs, Prp and Sps for andradite, grossular, pyrope and spessartine in garnet; Hem for hematite, Phl for phlogopite in mica and Prg for pargasite in amphibole. The simplest potentially useful equilibria are the one-site exchange:

$$MgMn_{-1}: Di + Sps = Jh + Prp$$

the coupled exhange:

$$(NaSi)(CaAl)_{-1}: Ae + An = Es + Ab$$

and the same exchange between plagioclase and scapolite. However, we note that end-member thermodynamic data are not yet available for esseneite and johanssenite clinopyroxenes. The stability of calcic scapolite end-members was investigated experimentally by Newton and Goldsmith (1975, 1976) and Goldsmith and Newton (1977). Pure meionite was found to decompose nearly isothermally to anorthite + calcite at 875ºC in reversed experiments:

$$Me = 3An + Cc$$

whereas silvialite was found to be stable at high pressure and high temperature relative to anorthite + anhydrite. The equilibrium is at 1040ºC at 1 bar, and has a slope of −48 bar/ºC (Goldsmith and Newton, 1977). Reversed experimental data obtained for meionite by Baker and Newton (1994) agreed with that of Goldsmith and Newton (1977) and allowed derivation of thermodynamic data for pure meionite. However, incorporation of a marialite component of scapolite is important in stabilizing it to lower temperature, and the plagioclase-scapolite exchange should provide a good thermometer. Aitken (1983) demonstrated that a Cl-free scapolite with Ca/(Na+Ca) = 0.83 underwent reversed vapour-absent breakdown to plagioclase + calcite at a lower temperature between 600ºC and 625ºC and 5 kbar. Unfortunately, attempts by Goldsmith and Newton (1977) to calibrate the thermometer gave unrealistically high T for assemblages containing intermediate or sodic plagioclase. This appears to be due to the complex activity-ordering-composition behaviour of both plagioclase and scapolite. The studies of Oterdoom and Gunter (1983) and Baker and Newton (1995) make it apparent that in the presence of excess calcite, the scapolite field extends to the lowest temperature for a composition near 'mizzonite', and scapolite can co-exist with two different plagioclase fields, one more calcic than the scapolite and the other more sodic. The scapolite and the plagioclase of this study are an example of the latter type, and have compositions broadly consistent with T = 550–600ºC in Fig. 2 of Baker and Newton (1995), even though that figure is compiled for $P = 0.7$ GPa.

Beryllium is almost identical in size to silicon but has only half the positive charge, and hence has a strong tendency to order in silicate frameworks (Hawthorne and Huminicki, 2002; Grew, 2002), so the structural state of the scapolite of this study needs to be determined before a reasonable activity model for it can be constructed.

In principle, the coexistence of the compositionally related volatile-rich minerals epidote and scapolite allows independent calculation of the f_{CO_2}/f_{H_2O} ratio in the associated fluid from the equilibrium:

$$Me + H_2O = 2Czo + CO_2$$

where Czo is the clinozoisite ($Ca_2Al_3Si_3O_{12}(OH)$) component in epidote.

The following net-transfer reactions involve pyroxene, amphibole, feldspar and garnet end-members:

(1) $An + Di + Ae = Ab + {}^1/_2Adr + {}^1/_3Prp + {}^1/_6Grs$

(2) $Kfs + Prg = Ab + Phl + {}^2/_3Grs + {}^1/_3Prp$

(3) ${}^3/_2Di + Hem + {}^1/_2Grs = Adr + {}^1/_2Prp$

Thermodynamic properties for the end-members and hence ΔG for the reactions were calculated over the range 300−800ºC and 0−5 kbar using THERMOCALC (Holland and Powell 1998).

It was found that contours of equal K for the three net-transfer reactions had very different P-T slopes: −0.24 kbar/100ºC, −1.8 kbar/100ºC and −11 kbar/100ºC, respectively. Therefore, they showed potential for very tight constraint of both temperature and pressure. However, reactions 1 and 3 gave implausibly low temperatures and pressures, while reaction 2 gave implausibly high estimates, possibly due to disequilibrium between phases. We note that the only {Fe, Mg, Mn}-rich phases to be observed in contact were the amphibole and mica. Garnet-pyroxene contacts have not been observed to date, although the homogeneous compositions of these minerals suggest that they have undergone little re-equilibration since growth.

Conclusions

We present a petrographic and mineralogical characterization of a new type of skarn from Långban, which is essentially a two feldspar-scapolite-spessartine-romeite granofels. The romeite shows substantial solid solution towards end-members containing Fe^{3+}, Ti and Sb^{3+}. The overall bulk composition and high degree of enrichment in Pb, Sb and As suggests that one of the precursors of the rock was a pre-existing Mn skarn. The Na, K and Be content suggest that this skarn reacted with a pegmatitic fluid derived from a potassic granite, with loss of silica, alkalis and CO_2. Very low sulphur and relatively high oxygen activities have allowed Pb and Sb to behave in a lithophilic fashion, entering oxide and (in the case of Pb) silicate minerals. The alkali and plagioclase feldspars and the scapolite have the highest Pb contents recorded in nature to date, and significantly extend the known geochemical possibilities for Pb under sufficiently low-f_{S_2} conditions. The scapolite also shows the highest known Be content for any scapolite. The ability of scapolite to act as principal repository for Be in {Ca,Al,CO_2}-rich metamorphic rocks is a new observation.

The observed mineralogy is consistent with the previously published regional peak conditions of P = 3 kbar, T > 600ºC. Several potential thermobarometers are identified in this rock, but there is as yet insufficient experimental calibration for these to be usable. Acquisition of thermodynamic data for a few Mn^{2+}- and Fe^{3+}-dominant silicate end-members would vastly improve our ability to obtain thermobarometric estimates for Mn-rich skarns. However, exsolution textures observed in many of the minerals of this rock imply that solid solutions are very non-ideal. Coexisting exsolved phases have been observed in the alkali feldspar, epidote, pyrochlore and apatite group minerals. The solutions that show exsolution involves exchange between cations with stereochemically active lone pairs (Pb^{2+}, Sb^{3+}) and without lone pairs (K, Ca, Ba), so non-ideality is likely to be enhanced by coupling between compositional variation and ordering, site splitting or distortion of coordination polyhedra (cf. Christy *et al.* 1998; Rouse *et al.* 1998). The closure temperatures for the solvi are minimum temperature estimates for the rock, but are unknown at present. Scapolite does not show exsolution but contains substantial Pb and also Be, which is known to show a strong tendency to order in other silicates (Grew, 2002). Evidently, crystal structural characterization and understanding of activity-composition relationships for the solid solutions is required, in addition to end-member thermodynamic properties, before the phase equilibria in a rock such as this skarn can be modelled with confidence.

Acknowledgements

We thank Sally Stowe and Frank Brink of the Electron Microscope Unit, ANU, for facilitating access to the unit, and also Roger Mason, Peter Scott and an anonymous referee for their reviews, which greatly improved this paper.

References

Aitken, B.G. (1983) Temperature-xCO_2 stability relations and phase equilibria of a calcic carbonate scapolite. *Geochimica et Cosmochimica Acta*, **47**, 351–362.

Baker, J. and Newton, R.C. (1994) Standard thermodynamic properties of meionite, $Ca_4Al_6Si_6O_{24}CO_3$, from experimental phase equilibrium data. *American Mineralogist*, **79**, 474–484.

Baker, J. and Newton, R.C. (1995) Experimentally determined activity-composition relations for Ca-rich scapolites in the system $CaAl_2Si_2O_8$-$NaAlSi_3O_8$-$CaCO_3$ at 7 kbar. *American Mineralogist*, **80**, 744–751.

Barthelemy, D. (2000) WWW Mineral Database: http://www.webmineral.com (accessed July 2005).

Belokoneva, E.L., Sokoleva, N.V. and Urusov, V.S. (1993) Scapolites – crystalline structures of marialite (Me_{11}) and meionite (Me_{88}) – spatial group as a function of composition. *Kristallografiya*, **38**, 52–77.

Benna P., Tribaudino M. and Bruno E. (1996) The structure of ordered and disordered lead feldspar ($PbAl_2Si_2O_8$). *American Mineralogist*, **81**, 1337–1343.

Berlepsch, P., Armbruster, T., Brugger, J., Criddle, A.J. and Graeser, S. (2003) Tripuhyite, $FeSbO_4$, revisited. *Mineralogical Magazine*, **67**, 31–46.

Brugger, J., Gieré, R., Graeser, S. and Meisser, N. (1997) The crystal chemsitry of roméite. *Contributions to Mineralogy and Petrology*, **127**, 136–146.

Carmichael, I.S.E., Turner, F.J. and Verhoogen, J. (1974) *Igneous Petrology*. McGraw Hill, New York, 739 pp.

Čech, F., Mosar, Z. and Povondra, P. (1971) A green lead-containing orthoclase. *Tschermaks Mineralogische und Petrologische Mitteilungen*, **15**, 213–231.

Černý, P., Smith, J.V., Mason, R.A. and Delaney, J.S. (1984) The geochemistry and petrology of feldspar crystallization in the Vežná pegmatite, Czechoslovakia. *The Canadian Mineralogist*, **22**, 631–651.

Christy, A.G. and Grew, E.S. (2004) Synthesis of beryllian sapphirine in the system MgO-BeO-Al_2O_3-SiO_2-H_2O and comparison with naturally occurring beryllian sapphirine and khmaralite, Part 2: A chemographic study of Be content as a function of P, T, assemblage and $FeMg_{-1}$ exchange. *American Mineralogist*, **89**, 327–338.

Christy, A.G., Grew, E.S., Mayo, S.C., Yates, M.G. and Belakovskiy, D.I. (1998) Hyalotekite, (Ba, Pb, $K)_4(Ca,Y)_2(B,Be,Si)_4Si_8O_{28}F$, a tectosilicate related to scapolite: new structure refinement, possible phase transitions and a short-range ordered 3*b* superstructure. *Mineralogical Magazine*, **62**, 77–92.

Christy, A.G., Tabira, Y., Hölscher, A., Grew, E.S. and Schreyer, W. (2002) Synthesis of beryllian sapphirine in the system MgO-BeO-Al_2O_3-SiO_2-H_2O and comparison with naturally occurring beryllian sapphirine and khmaralite, Part 1: Experiments, TEM and XRD. *American Mineralogist*, **87**, 1104–1112.

Deer, W.A., Howie, R.A., Wise, W.S. and Zussmann, J. (2004) *Rock-Forming Minerals, Volume 4B: Silica Minerals, Feldspathoids and the Zeolites* (2^{nd} edition). The Geological Society, London.

Dunn, P.J. (1995) *Franklin and Sterling Hill, New Jersey: the World's Most Magnificent Mineral Deposits*. Published by the author.

Filatov, S.K., Krivovichev, S.V., Burns, P.C. and Vergasova, L.P. (2004) Crystal structure of filatovite, $K(Al,Zn)_2(As,Si)_2O_8$, the first arsenate of the feldspar group. *European Journal of Mineralogy*, **16**, 537–544.

Gillberg, M. (1960) A lead-bearing variety of pargasite from Långban, Sweden. *Arkiv för Mineralogi och Geologi*, **2**, 425–430.

Goldsmith, J.R. and Newton, R.C. (1977) Scapolite-plagioclase stability relationships at high pressures and temperatures in the system $NaAlSi_3O_8$-$CaAl_2Si_2O_8$-$CaCO_3$-$CaSO_4$. *American Mineralogist*, **62**, 1063–1081.

Grew, E.S. (2002) Beryllium in metamorphic environments (emphasis on aluminous compositions). Pp. 487–549 in: *Beryllium: Mineralogy, Petrology and Geochemistry* (E.S. Grew, editor). Reviews in Mineralogy and Geochemistry, **50**. Mineralogical Society of America, and the Geochemical Society, Washington, D.C.

Hassan, I. and Buseck, P.R. (1988) HRTEM characterization of scapolite solid solutions. *American Mineralogist*, **73**, 119–134.

Hawthorne, F.C. (2002) The use of end-member charge arrangements in defining new species and heterovalent substitutions in complex minerals. *The Canadian Mineralogist*, **40**, 699–710.

Hawthorne, F.C. and Huminicki, D.M.C. (2002) The crystal chemistry of beryllium. Pp. 333–444 in: *Beryllium: Mineralogy, Petrology and Geochemistry* (E.S. Grew, editor). Reviews in Mineralogy and Geochemistry, **50**. Mineralogical Society of America, and the Geochemical Society, Washington, D.C.

Holland, T.J.B. and Powell, R. (1998) An internally consistent thermodynamic data set for phases of petrological interest. *Journal of Metamorphic Geology*, **16**, 309–343.

Holtstam, D. and Langhof, J. (1994) Hancockite from Jakobsberg, Filipstad, Sweden: the second world occurrence. *Mineralogical Magazine*, **58**, 172–174.

Holtstam, D. and Langhof, J. (1999) *Långban: the Mines, their Minerals, Geology and Explorers*. Raset Förlag, Swedish Museum of Natural History, Stockholm.

Holtstam, D., Nysten, P. and Gatedal, K. (1998) Parageneses and compositional variations of Sb oxyminerals from Långban-type deposits in Värmland, Sweden. *Mineralogical Magazine*, **62**, 395–407.

International Mineralogical Association (1998) *The nomenclature of minerals: a compilation of IMA reports*. Pp.148–149: *Appendix: symbols of the rock-forming minerals*. http://www.mineralogicalassociation.ca/doc/abstracts/ima98/ima98.htm.

Jambor, J.L and Roberts, A.C. (1997) New mineral names. *American Mineralogist*, **82**, 1261–1264.

Kalt, A., Schreyer, W., Ludwig, T., Prowatke, S., Bernhardt, H.-J. and Ertl, A. (2001) Complete solid solution between magnesian schorl and lithian excess-boron olenite in a pegmatite from the Koralpe (eastern Alps, Austria). *European Journal of Mineralogy*, **13**, 1191–1205.

Levien, L. and Papike, J.J. (1976) Scapolite crystal chemistry: aluminum-silicon distributions, carbonate group disorder, and thermal expansion. *American Mineralogist*, **61**, 864–877.

Lin, S.B. and Burley, B.J. (1973*a*) Crystal structure of a sodium- and chlorine-rich scapolite. *Acta Crystallogaphica*, **B29**, 1272–1278.

Lin, S.B. and Burley, B.J. (1973*b*) The crystal structure of meionite. *Acta Crystallogaphica*, **B29**, 2024–2026.

Lin, S.B. and Burley, B.J. (1975) The crystal structure of an intermediate scapolite-wernerite. *Acta Crystallogaphica*, **B31**, 1806–1814.

Lindqvist, B. and Charalampides, G. (1987) Stability and kinetic studies of synthetic solid solutions in the kentrolite-melanotekite series. *Geologiska Föreningens i Stockholm Förhandlingar*, **109**, 73–82.

Mason, R.A. (1982) Trace-element distributions between the perthite phases of alkali feldspars from pegmatites. *Mineralogical Magazine*, **45**, 101–106.

Matsubara, S., Kato, A., Shimizu, M., Sekiuchi, K. and Suzuki, Y (1996) Roméite from the Gozaisho mine, Iwaki, Japan. *Mineralogical Journal*, **18**, 155–160.

McSwiggen, P.L., Morey, G.B. and Cleland, J.M. (1994) Occurrence and genetic implications of hyalophane in manganese-rich iron formation. *Mineralogical Magazine*, **58**, 387–399.

Mellini, M. and Merlino, S. (1979) Versiliaite and apuanite – derivative structures related to schafarzikite. *American Mineralogist*, **64**, 1235–1242.

Mellini, M., Merlino, S. and Orlandi, P. (1979) Versiliaite and apuanite, 2 new minerals from the Apuan Alps, Italy. *American Mineralogist*, **64**, 1230–1234.

Moore, P.B. (1970) Mineralogy and chemistry of Långban-type deposits in Bergslagen, Sweden. *Mineralogical Record*, **1,** 154–172.

Newton, R.C. and Goldsmith, J.R. (1975) Stability of scapolite meionite ($3CaAl_2Si_2O_8.CaCO_3$) at high pressures and storage of CO_2 in deep crust. *Contributions to Mineralogy and Petrology*, **49**, 49–62.

Newton, R.C. and Goldsmith, J.R. (1976) Stability of end-member scapolites – $3NaAlSi_3O_8.NaCl$, $3CaAl_2Si_2O_8.CaCO_3$, $3CaAl_2Si_2O_8.CaSO_4$. *Zeitschrift für Kristallographie*, 143, 333–353.

Oterdoom, W.H. and Gunter, W.D. (1983) Activity models for plagioclase and CO_3-scapolites: an analysis of fluids and laboratory data. *American Journal of Science*, **283-A** (Orville volume), 255–283.

Papike, J.J. and Stephenson, N.C. (1966) The crystal structure of mizzonite: a calcium- and carbonate-rich scapolite. *American Mineralogist*, **51**, 1014–1027.

Papike, J.J. and Zoltai, T. (1965) The crystal structure of a marialite scapolite. *American Mineralogist*, **50**, 641–655.

Perseil, E.-A. and Smith, D.C. (1995) Sb-rich titanite in the manganese concentrations at St Marcel-Praborna, Aosta Valley, Italy: Petrography and crystal-chemistry. *Mineralogical Magazine*, **59**, 717–734.

Phakey, P.P. and Ghose, S. (1972) Scapolite: observation of an antiphase domain structure. *Nature Physical Science*, **238**, 78–80.

Plimer, I.R. (1976) A plumbian feldspar pegmatite associated with the Broken Hill orebodies, Australia. *Neues Jahrbuch für Mineralogie Monatshefte*, 272–288.

Rouse, R.C., Dunn, P.J., Peacor, D.R. and Wang, L. (1998) Structural studies of the natural antimony pyrochlores 1. Mixed-valency, cation site splitting, and symmetry reduction in lewisite. *Journal of Solid State Chemistry*, **141**, 562–569.

Seto, Y., Shimobayashi, N., Miyake, A. and Kitamura, M. (2004) Composition and $I4/m$-$P4_2/m$ phase transition in scapolite solid solutions. *American Mineralogist,*, 89, 257–265.

Shannon, R.D. (1976) Revised effective ionic radii and systematic studies of interatomic distances in halides and chalcogenides. *Acta Crystallographica*, **A32**, 751–767.

Sherriff, B.L., Sokolova, E.V., Kabalov, Y.K., Jenkins, D.M., Kunath-Fandrei, G., Goetz, S., Jäger, C. and Schneider, J. (2000) Meionite: Rietveld structure-refinement, ^{29}Si MAS and ^{29}Al SATRAS NMR spectroscopy, and comments on the marialite-meionite series. *The Canadian Mineralogist,*, 38, 1201–1213.

Smith, D.C. and Perseil, E.-A. (1997) Sb-rich rutile in

the manganese concentrations at St. Marcel-Praborna, Aosta Valley, Italy: petrography and crystal chemistry. *Mineralogical Magazine*, **61**, 655–669.

Smith, J.V. and Brown, W.L. (1988) *Feldspar Minerals* (2^{nd} edition, revised and extended) vol. 1: Crystal Structures, Physical, Chemical and Microtextural Properties. Springer-Verlag, Berlin, Heidelberg, New York, London, Paris, Tokyo.

Steele, I.M., Hutcheon, I.D. and Smith, J.V. (1977) Ion microprobe analysis of plagioclase feldspar ($Ca_{1-x}Na_xAl_{2-x}Si_{2+x}O_8$) for major, minor and trace elements. Pp. 515–525 in: *8^{th} International Congress on X-ray Optics and Microanalysis*. Pendell Publishing Co., Midland, MI, USA.

Stevenson, R.K. (1985) An occurrence of amazonite, gahnite and sphalerite near Portman Lake, Northwest Territories. *Geological Survey of Canada Paper*, **85-1A**, 23–28.

Stevenson, R.K. and Martin, R.F. (1986) Implications of the presence of amazonite in the Broken Hill and Geco metamorphosed sulfide deposits. *The Canadian Mineralogist*, **24**, 729–745.

Stevenson, R.K. and Martin, R.F. (1988) Amazonitic K-feldspar in granodiorite at Portman Lake, Northwest Territories: indications of low $f(O_2)$, low $f(S_2)$ and rapid uplift. *The Canadian Mineralogist*, **26**, 1037–1048.

Teertstra, D.K. and Sherriff, B.L. (1996) Scapolite cell-parameter trends along the solid-solution series. *American Mineralogist,*, 81, 169–180.

Teertstra, D.K. and Sherriff, B.L. (1997) Substitutional mechanisms, compositional trends and the end-member formulae of scapolite. *Chemical Geology*, **136**, 233–260.

Teertstra, D.K., Schindler, M., Sherriff, B.L. and Hawthorne, F.C. (1999) Silvialite, a new sulfate-dominant member of the scapolite group with an Al-Si composition near the $I4/m$-$P4_2/n$ phase transition. *Mineralogical Magazine*, **63**, 321–329.

Vergasova, L.P., Krivovichev, S.V., Britvin, S.N., Burns, P.C. and Ananiev, V.V. (2004) Filatovite, $K(Al,Zn)_2(As,Si)_2O_8$, a new mineral species from the Tolbachik volcano, Kamchatka peninsula, Russia. *European Journal of Mineralogy*, **16**, 533–536.

[*Manuscript received 28 August 2004: revised 12 October 2005*]